REPORT DOCUMENTATION PAGE

AFRL-SR-AR-TR-05-

0523

1. REPORT DATE	2. REPORT TYPE	3. DATES COVERED
12-12-2005	Final Performance Report	Apr 2002 – Oct 2005

4. TITLE AND SUBTITLE

Model Development and Verification of the CRIPTE code for Electromagnetic Coupling

5a. CONTRACT NUMBER

5b. GRANT NUMBER
F 49620-02-1-0183

5c. PROGRAM ELEMENT NUMBER

6. AUTHOR(S)

Naz E. Islam
Phumin Kirawanich
Lab personnel

5d. PROJECT NUMBER

5e. TASK NUMBER

5f. WORK UNIT NUMBER

7. PERFORMING ORGANIZATION NAME(S) AND ADDRESS(ES)

ECE Department
University of ~~Missouri~~ New Mexico
319, Engineering Building West
Columbia, MO 65211

8. PERFORMING ORGANIZATION REPORT NUMBER

9. SPONSORING / MONITORING AGENCY NAME(S) AND ADDRESS(ES)

AFOSR
875 North Randolph Street
Suite 325
Arlington VA, 22203-1768

10. SPONSOR/MONITOR'S ACRONYM(S)

AFRL

11. SPONSOR/MONITOR'S REPORT NUMBER(S)

12. DISTRIBUTION / AVAILABILITY STATEMENT

Distribution Statement A: unlimited

13. SUPPLEMENTARY NOTES

14. ABSTRACT

Topological simulation methods for EM-system interactions were studied using the topological code CRIPTE (made available through AFRL, NM). A definition of simulation based transfer function in topological codes has evolved as a result of this study which was later used in topological based simulations for CAT-5 cables and twisted pairs interactions. Electromagnetic effects studies also include RF heating of electrical devices, as well the transmission of electromagnetic energy the active region of a metal-semiconductor-metal detector. This effort has resulted in the publication of twenty five (25) Journal articles, book chapter and conference proceedings. Our collaborative work has been presented at the classified sessions of the five-power Air Senior National Representative (ASNR) High Power Microwave Meeting and the Directed Energy Professional Society (DEPS) High Power Microwave Conference.

15. SUBJECT TERMS

16. SECURITY CLASSIFICATION OF:			17. LIMITATION OF ABSTRACT	18. NUMBER OF PAGES	19a. NAME OF RESPONSIBLE PERSON
a. REPORT	b. ABSTRACT	c. THIS PAGE			19b. TELEPHONE NUMBER *(include area code)*

FINAL REPORT

April 2002-October2005

Model Development and Verification of the CRIPTE code for Electromagnetic Coupling

AFOSR Grant F49620-02-1-0183

Principal Investigator

Naz E. Islam, PhD
Associate Professor

Based on contributions from

Phumin Kirawanich, PhD
And
Graduate and Undergraduate Students who have worked on the projects

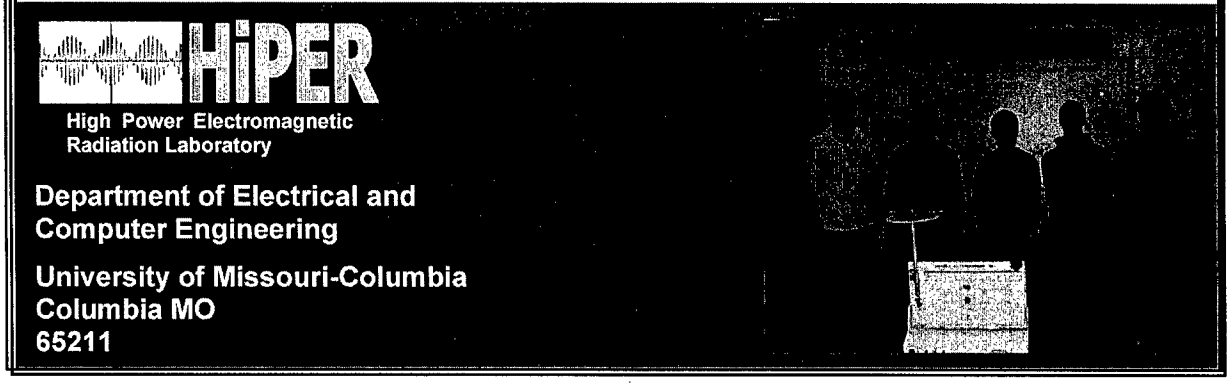

Model Development and Verification of the CRIPTE code

PI: Naz Islam
University of Missouri-Columbia
AFOSR Grant F49620-02-1-0183

Summary

This report summarizes our research work for the duration of the AFOSR Grant # F49620-02-1-0183. Due to the PI's move from the University of New Mexico, NM to the University of Missouri in Columbia (UMC), Missouri, in August 2003, there was a transition period of relative inactivity and therefore the effort was extended to October 2005, at no cost to AFOSR. This effort has resulted in the publication of twenty five (25) Journal articles, book chapter and peer reviewed conference proceedings (page 76). A fully developed research facility with both computational and experimental facility including EMC tester for irradiating samples, spectrum analyzer, network analyzer, near field and other probes and a Gyrotron has been setup with the AFOSR grant support and collaboration with faculties at ECE, UMC. A total of 21 graduate and undergraduates (a majority with US citizenship) have been trained in the HiPER (High Power Electromagnetic Radiation) Laboratories.

The basic objective of the research project was to study topological simulation methods, using the topological code CRIPTE. This initial effort has contributed to the definition of simulation based transfer function in topological codes. The transfer function is an important tool necessary for aperture interaction simulations, and the subsequent interactions of an electromagnetic pulse with cables, and circuitry inside a semi-shielded system. We have proposed three different methodologies for such transfer function generation, including a quasi approach that utilizes part experimental results.

In the research period we have also looked into topological based simulations for CAT-5 cables and twisted pairs, where topological method to minimize cross talk is discussed. Electromagnetic effects studies also include RF heating of semi-conductor devices, as well the transmission of electromagnetic energy through the nano grating structures on the active region of a metal-semiconductor-metal detector. Work on the detector is collaboration with VSSE AFRL/NM, while the bulk of our research is collaboration with DE/HE, NM. Our collaborative work has been presented at two classified sessions, e. g. The Five-power (US, UK, Germany, France and Italy) Air Senior National Representative (ASNR) High Power Microwave Meeting, held 14-17 February 2005 at Eglin AFB, FL. And the Directed Energy Professional Society (DEPS) High Power Microwave Conference, held 17-19 August 2004 in Albuquerque

We have continued our effort in RF effects studies through a follow up proposal and have established a close collaboration with DEHE/AFRL, NM as well as other faculty members at the Electrical and Computer Engineering and other Departments at MU. Besides the simulation laboratory we have also established an experimental facility for RF effects studies and hope to extend research into studying the effects of electromagnetic radiation on biological systems and plant genetics. This effort is expected to be a close collaboration with the life science faculties at UMC, Old Dominion University, University of Michigan and AFRL/Brooks are also expected to participate.

Model Development and Verification of the CRIPTE code

PI: Naz Islam
University of Missouri-Columbia
AFOSR Grant F49620-02-1-0183

TABLE OF CONTENTS

Model Development and Verification of the CRIPTE code

PI: Naz Islam
University of Missouri-Columbia
AFOSR Grant F49620-02-1-0183

I. INTRODUCTION

This report summarizes research activities for AFOSR Grant # F49620-02-1-0183, by faculties and students at the University of Missouri-Columbia (UMC). A part of the research was conducted at the University of New Mexico (UNM), Albuquerque, NM before the PI moved to UMC. We have continued to concentrate our research effort on the implementation of the topological code (CRIPTE), model development and training of manpower. On the experimental studies we have worked on measuring scattering parameters of the computer network card and parameters related to format conversion in the code. Recently, we have also started work on experiments related to radiation from cable, propagation trough apertures in close collaboration with AFRL New Mexico. The overall research objective has been to characterize the effects of high frequency electromagnetic radiation on cables and electrical systems.

The effects of radio frequency pulses on electronic systems such as network cables connecting critical elements in a system can probably cause the system temporary or permanent damage. Such critical elements have been defined as network computers connected through the cables. The cables interact with the computers through the network cards. The potential vulnerability of the electronic systems has motivated our research group to study the network system behaviors under this circumstance. The objective is to measure the scattering matrix for the network card at various operating states. The data from the experiment will then be input to the state of the art computer code (CRIPTE) having multiconductor transmission line network (MTLN) as its application domain. The CRIPTE code is based on the Electromagnetic Topology (EMT) theory, initially presented by AFRL, NM.[1,2] The network defined through the code will thus consist of cable lines connected through junctions. The junctions here represent computers. The measured S-parameters will then be fed into the junctions as input and the network comprising of junctions and cables

will be analyzed for RF effects by introducing external RF sources on the cable network. The modules developed for RF effects can then be used for the analysis of critical parameters pertinent to more complex systems. This initial study will thus become the building block for analyzing more complex systems linked through above ground or underground cables. An example of such a complex system is a cable network connecting different buildings that house important electronics or information database systems.

A number of researches including US nationals (section IV) are contributing to the research effort at both UMC and AFRL. The research is being complemented through FDTD based simulations and semiconductor device and circuit simulations for EMP interactions. The results obtained can be integrated into the CRIPTE network simulation for larger volumes. Understanding the effects of EMP on systems and devices is expected to lead to predictive capabilities, which will ultimately in shielding studies against such effects. The research effort has also resulted in a number of journal and conference publications and interactions with peers and DoD personnel conducting research in this area (sections V and VI(a)).

II. TRAININGS AND SETUPS

(A) Intensive Short Course HPE 201-03 by Dr. Carl E. Baum

As a part of a work continuation on the first project, i.e. Implementation of the topological code and Training of manpower, during the week of 27 July – 2 August 2003, Dr. Phumin Kirawanich attended a one week intensive short course on High-Power Electromagnetics: Environments, Interaction, Effects, and Hardening (HPE 201-03) at New Mexico Tech, Socorro, NM, USA, sponsored by SUMMA Foundation. This course, conducted by Dr. Carl E. Baum, who is also a president of SUMMA Foundation, is designed to

familiarize students who have a good electromagnetic background with fundamentals of HPE, including sources, interaction, effects, and hardening. Very important is the student participation via presentation of problem assignments and solutions. The course participants include twenty-six students, forming six of four and five-people groups, and five faculty members from leading HPE experts in the USA and Europe. A large portion of the course was devoted to the lectures given by faculty members on selected aspects of HPE. At the end of each lecture, a related problem assignment will be given out to a group who has a special interest on that subject area. Each student in the group will give a mini-lecture on the task assigned. Also, Dr. Phumin Kirawanich spent some time with Dr. Parmantier to get himself familiar with the CRIPTE code as it is the major tool of the research conducted at UMC.

Lecture Content

Regarding the research effort at UMC on the effects of radio frequency pulses on network cables, the lecture relevant to the on-going project was given by Dr. Parmantier. His lecture consists of two main topics: the Applied EM Topology and EM coupling on cable networks. The detail of the Applied EMT includes the topological analysis and topological networks. The objective of this topic is to provide an operational vision of the theory in order to structure an analysis for assessing EM coupling on a complex system based on topological diagram and graph approaches. It also intends to show the concept of a network representation using the network terminology, such as junctions and tubes, and the BLT equation describing all the network connections. In addition, the lecture of EM coupling on cable networks gives the basic ideas and examples of modeling the transmission line and EM coupling using various techniques for different types of network cables.

Problem Assignment and Solution (theoretical and numerical analysis approaches)

The course perception was evaluated through how well in using the material obtained during the course lecture to exercise on the assigned task. The group effort will be very

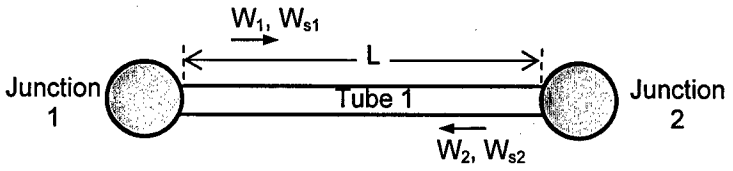

Fig. IIA-1 Topological network made of one tube and two junctions.

important at this step. Group members will then be presenting their parts of the assignment. Nevertheless, a simplified-theoretical analysis approach, as a time was limited, can only give a brief solution. Hence, the resulting solutions will be verified with the corresponding results from a numerical analysis obtained by the tools such as LAPLACE and CRIPTE codes. This part needs to carry out at UMC where the program codes were implemented on the SUN workstation (SUNBlade 2000).

Fig. IIIA-1 shows a one-tube, two-junction topological network as the network system considered in the assignment. Note that this setup also corresponds to the computer network system shown in Fig. IIA-1 where the junctions and tube represent the network cards and the transmission cable, respectively. The objectives of the assignment are as follows:

1. Practice the building of the BLT equation on a simple network.
2. Use the solution to analyze the response of two specific wiring problems: short-circuited open cable and matched coaxial cable.
3. Link the two elementary problems through a transfer impedance to solve a shielded cable problem.
4. Other topics: different aspects of TL matching, equivalent electric circuit at low frequency, and cable resonances.

Fig. IIA-2(a) shows theoretically the current response as a function of a frequency when the network consists of a one-wire transmission line short-circuited at both ends (a

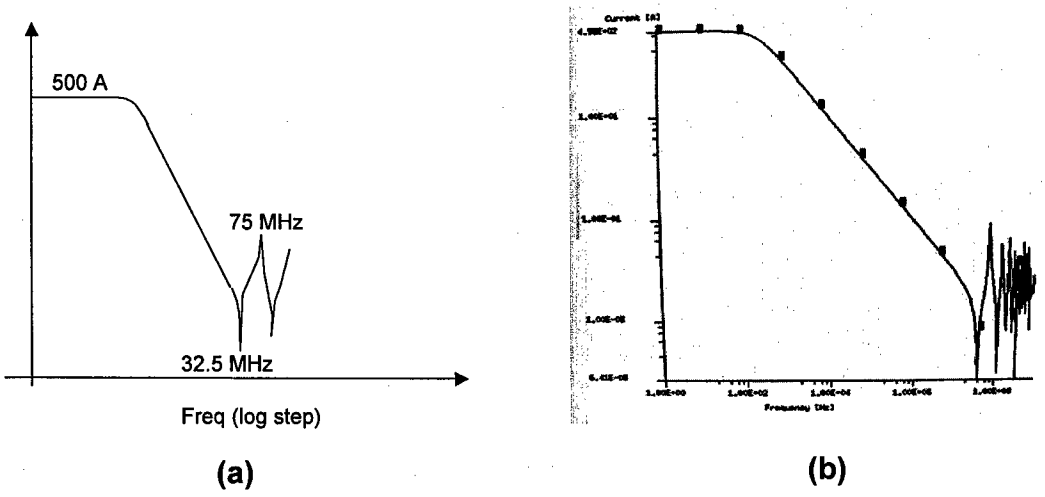

Fig. IIA-2 Current response on the short-circuited transmission line by (a) theoretical analysis and (b) CRIPTE code.

single conductor cable over a ground plane). The corresponding result using the CRIPTE code can be seen in Fig. IIA-2(b). The good agreement shows the capabilities of the CRIPTE code in studying the characteristics of the network cables under various conditions.

(B) HiPER Topological Simulations (CRIPTE)

We continue our focus on developing topological schemes for EMP-electrical systems interactions by launching HiPER (High Power Electromagnetic Radiation) laboratory for the research CRIPTE code at UMC. An understanding of the code has led to the development of new models and concepts that can be implemented in various interaction schemes. Our current effort at the ECE department, UMC has contributed significantly to the understanding of topological schemes for aperture interactions and the results obtained have been documented and updated for use at DE/AFRL, NM.

System Description

At the ECE effect laboratory, the RORQUAL, LAPLACE and CRIPTE codes were implemented on a LINUX server (RedHat 9.0, Dell Xeon). Connected to the server are two

workstations (WINXP, Dell Pentium 4) that can run the program on the host independently through LAN network.

RORQUAL is the software allows the user to execute numurical operations on both real and complex signals on Time and Frequency domains. Many features are available such as basic operations, Fourier Transform, inverse Fourier Transformer, Fast Fourier Transform, inverse Fast Fourier Transform, etc.

LAPLACE is a numerical code, which handles the calculation of a multiconductor transmission line's impedance and admittance. The LAPLACE code solves by using the Method of Moments on the cross sectional geometry of the cable harnesses and the dielectric materials surrounding the cable conductors.

The CRIPTE simulation tool is the key to study the RF system interactions. By characterizing the tubes (cable parameters) using the output from the LAPLACE code and junctions from CRIPTE itself (impedance parameters) or measurement (S-parameters), the interaction can be performed.

General Description of Trainings Facilities and Problem Assignment

Weekly training sessions of basic topological simulations has been scheduled to provide the knowledge and skills to US national students as the part of the program objective. Their assignments were to solve the problems based on the real life situations and to compose the topological code user manual in English language.

David Gleason, a US national student, was supported by AFRL for an intern position at AFRL during June – August 2005. His work assignment mainly focused on the applications of a topological code on communication cables under external threats. The on-going work is a new development of the topological code in time domain.

(C) High Power Radiation Source (s) (HEIMDALL)

The Heimdall software is used to model and analyze radio frequency (RF) weapon systems. It is commonly used to examine the possible threat of potential and current foreign RF weapon systems. A user can either design his/hers own system with specific technologies or the software can create a weapon system based on a desired power density on a particular target. The RF weapon systems use high power microwave (HPM) devices as the source of electromagnetic radiation. The user has access to the performance and physical attributes of the entire system.

Before designing the RF weapons system, a platform and a target need to be designated. The platforms are where the RF weapons systems are contained in and can be chosen from a large selection of transport in aircraft, missiles, ground modules, and watercraft. The various platforms have specific weight and volume limitations that the RF systems must be confined. The targets of the weapons system can range from military sites such as anti-aircraft and missiles to infrastructure like personal computers and communications. The targets can specify there height and polarization are related to the weapons system and also there kill mechanism, which is how the target is disabled.

After specifying the platform, target, and components of the RF weapons system, the user can evaluate the system on the target. The power density and electric field can be measured based on the range of the target from the device. The other important feature of the software is the variety of analysis tools that allow the user to fine-tune the model along with the system performance.

Sample Model of RF Weapon System

In this section, a sample model is chosen with its platform, target and various technologies described in detail. The parameters of the technologies will be analyzed and

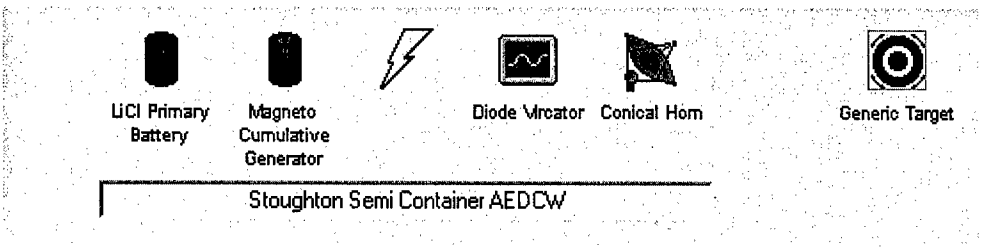

Fig. IIC-1 Heimdall representation of RF weapon system (Magnetocumulative Generator).

described along with the power density and electric field on the target. In Fig. IIC-1, this is how the model of a Magnetocumulative Generator looks in Heimdall.

Problem Assignment

A group of US citizen students was assigned to constitute the RF weapon system as a threatening EMP source to civilian power distribution system. The output from HEIMDALL will be incorporated with the topological code implementing the complete scenario of the power distribution grid under airborne weapon attacks.

(D) Electromagnetic Interaction with Devices and Structures (Silvaco, CST)

At the HiPER laboratory, we are studying new designs for semiconductor switches used in the generation of UWB HPM. RF heating of such devices is likely to effects its performance. In order to see such effects, simulations were carried out on switches fabricated from a number of materials, such as GaAs and SiC, that are likely to be used at AFRL. NM. The SILVACO software, which is a comprehensive package for semiconductor material, device and process simulation studies was used in this project. The software was installed on a LINUX server (RedHat 9.0, Dell Xeon). Connected to the server are two workstations (WINXP, Dell Pentium 4) that can run the program on the host independently through LAN network.

Alternate study focuses on semiconductor structures. The effects of different geometries, heights and concentrations per unit area of gratings in the active region of a semiconductor photo-detector have been analyzed for enhanced charge collection through electromagnetic field analysis. The CST Microwave studio software with floating licenses was installed on two servers (WINXP, Dell Pentium 4) connected to two client workstations (WINXP, Dell Pentium 4). This is a fully featured software package for Electromagnetic analysis and design in the high frequency range. After the component has been modeled, a fully automatic meshing procedure (based on expert system) is applied before the simulation engine is started. The simulators feature the Perfect Boundary Approximation (PBA method) and its Thin Sheet Technique (TST) extension, which increases the accuracy of the simulation by an order of magnitude in comparison to conventional simulators. The most flexible tool of this software is the transient solver, which can obtain the entire broadband frequency behavior of the simulated device from only one calculation run (in contrast to the frequency stepping approach of many other simulators). This solver is very efficient for most kinds of high frequency applications.

(E) In-House Simulations for Comparisons (FDTD)

When simulating external pulses interactions with internal electrical systems, EMT based simulations, require transfer function generation at the aperture. Field characteristics following aperture interactions have been studied. In our work, we compare such interactions using EMT method with results using the finite-difference time-domain (FDTD) algorithm. Both the FDTD and the EMT simulations were carried out on a Pentium XEON-processor Linux server. The 2D and 3D FDTD codes were implemented using the C program language.

(F) Simulation and Experimental Facilities

Simulation Laboratory

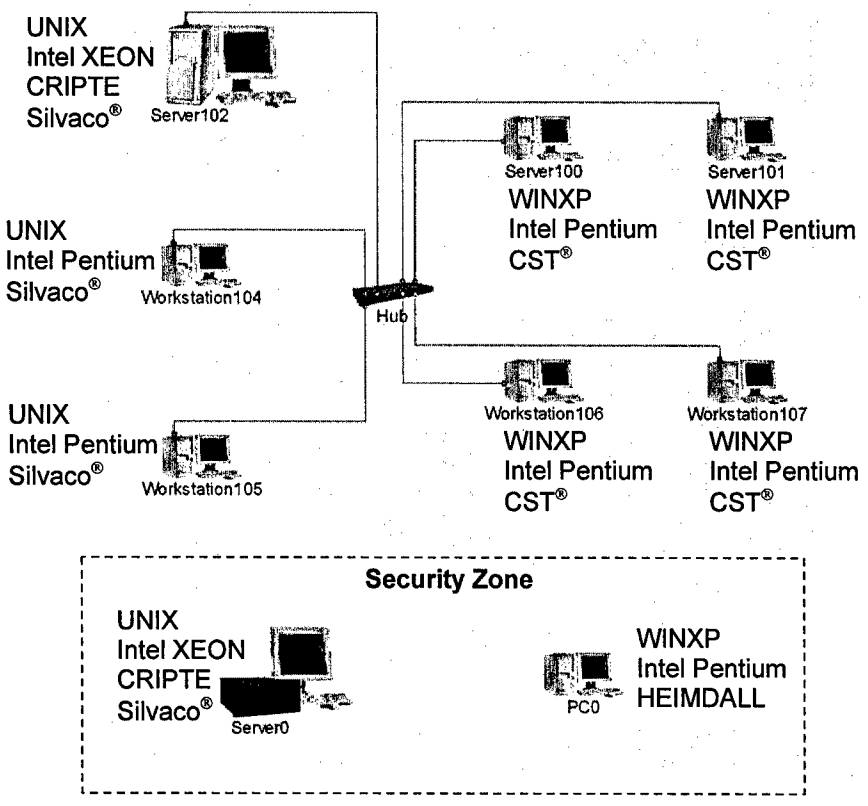

Fig. IIF-1 Computer simulation network at HiPER laboratory

At HiPER laboratory, two separate groups of electromagnetic computer based simulation and experimental validation are working correlatively. Fig. IIF-1 shows the diagram of the computer network setup the way to handle multiple users. There is also the isolated area for US national students.

Anechoic Chamber for Objects under Radiation/CRIPTE Validation

The High Power Electromagnetic Radiation (HiPER) Laboratory at the University of Missouri-Columbia (UMC) is involved in a collaborative effort with the Directed Energy Directorate, Air Force Research Laboratory (AFRL), NM, in the area of electromagnetic pulse interactions with electrical systems through an AFOSR supported grant. We have been

granted in the total amount of $173,000 to purchase equipments to conduct experiments in electromagnetic compatibility analysis of communication cables and its validation through electromagnetic topology based simulation code. The diagram and specification of the FS4010 system is shown in Fig. IIF-2. This system consists of the following; (i) RF amplifier, (ii) RF signal generator, (c) power meter, (d) RF system controller, (e) dual directional coupler, (f) isotropic E field probe, (g) current probes, (h) an anechoic test chamber, and (i) test accessories. Equipments are for the measurement of induced currents at different wiring of a network under electromagnetic excitation.

The system (Fig. IIF-3) will enable the researchers to perform an electromagnetic conducted and radiation susceptibility tests on cables and equipment under test (EUT). The EUT could be a critical component of larger platforms such as aircraft's electronic components, cables etc. The PI and his research team, in close collaboration with AFRL, NM are investigating electromagnetic interference effects on the cables of such systems using

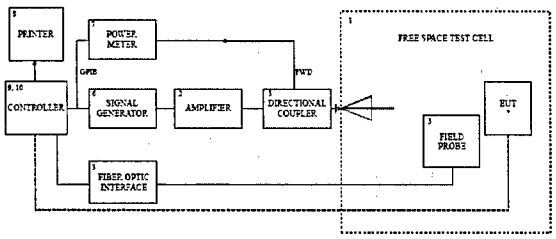

SYSTEM BLOCK DIAGRAM (IMMUNITY)

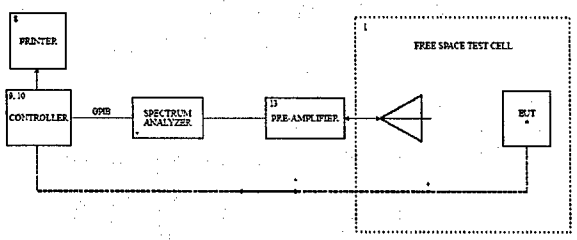

SYSTEM BLOCK DIAGRAM (EMISSIONS)

Frequency range	27 – 1000 MHz
Field strength	10 V / m max
Max DUT size	100×100 cm^2
Input RF power	150 Watts max
Cell dimension	$5.7 \times 2.6 \times 2.4$ m^3

Fig. IIF-2 FS4010 system.

computational tools based on topological simulation methods and aided by FDTD codes. However, to confirm the validity of the preliminary simulations, verification with measurement is very important. Measured data would either validate existing simulation models or suggest a necessary modification based on the physics involved. Preliminary work in this area was started at AFRL when the PI for this project and the support group was located at New Mexico who has since moved to U Missouri-Columbia.

The test system will greatly enhance the research capability to support the existing DOD programs at the RF Effect laboratory at the University of Missouri-Columbia. The system also adds a new dimension to the study of EMP interaction with electrical systems now being pursued at ECE laboratory at UMC. The measurements will enable the researchers to understand how seriously the external EMP and associated interactions can affect the critical systems. The code used for the analysis is based on topological simulation

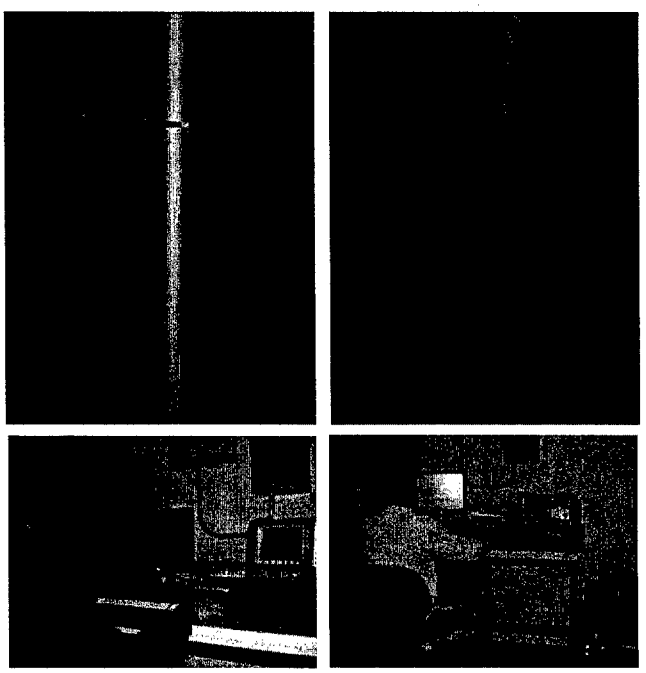

Fig. IIF-3 Chamber interior and control interface.

techniques, a research are now pursued at the AFRL, NM, and our collaborative partner.

Near Field Probe to Discriminate Objects

We plan to use the images from the near field probe to discriminate between objects. Work in this area has just started. Preliminary setups for identifying a washer through Horn Antenna pattern discrimination (Fig. IIF-4) is being studied.

GYROTRON Radiation Facility

We have also setup a Gyrotron (Fig. IIF-4) testing facility in collaboration with another faculty at ECE, MU. The test facility is a donation from the Los Alamos Laboratories, Albuquerque, NM.

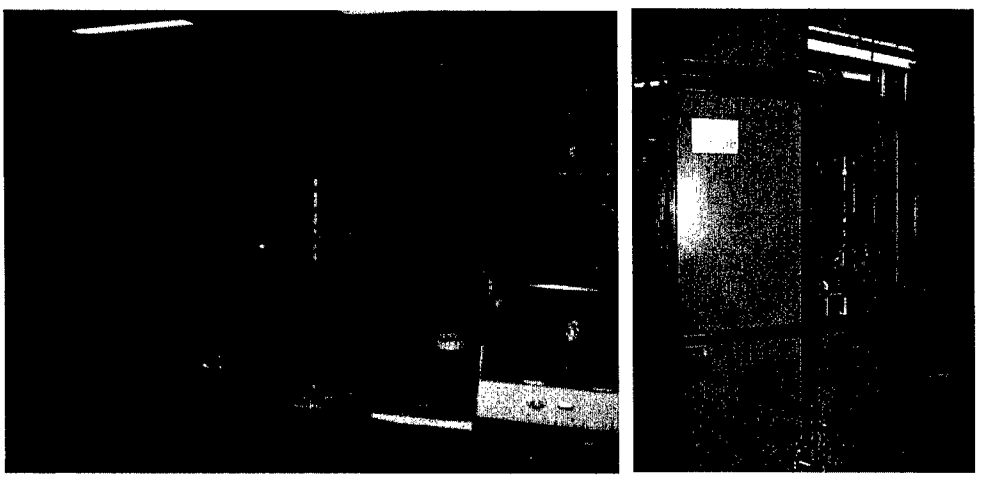

Fig. IIF-4 Near Field probe (left) and Gyrotron (right) at HiPER laboratory.

III. ACCOMPLISHMENTS ON EMP SUDIES

Our research effort was primarily dedicated to topological modeling using the CRIPTE code where new models for external-internal interactions were introduced. We

have also complemented this study with FDTD analysis for aperture interactions. Finally, we have looked into EMP heating of devices.

(A) Interaction Studies: Topological Approach (Introduction of Transfer Function)

Research at UMC has contributed greatly to the successful application of the electromagnetic based CRIPTE simulation tool, specifically in the area of external-internal coupling through an aperture. A new concept was introduced in the simulation tool where the external-internal interactions were treated through topological decomposition and a transfer function was generated through simulations, rather through experiments as was done previously. Such a scheme showed results that are consistent with experiments. The generated transfer function can be used in different interaction sequences of the topological code. The following sections detail the computer system configuration and summarize a highlight of activities such as, EMT volume decomposition, external field couplings, field penetration through openings, and internal cable propagation of induced signals through computer network analysis.

System Volume Decomposition

Fig. IIIA-1(a) is a very simplified aircraft system consisting of only two computer mainframes, connecting each other with a communication cable. By using EMT approach, the geometry of the entire system in Fig. IIIA-1(a) can be broken down in to three different volumes, i.e. V_0, V_1, and V_2 included within each other as described by the topological decomposition diagram shown in Fig. IIIA-1(b). It has an external volume V_0 covering the entire system. The external disturbance, say an EMP wave, upon penetrating the outer shielded surface $S_{0,1}$, radiates through the internal medium with ε_0 and μ_0 in volume V_1 and couples on the shielded surface $S_{1,2}$, which may represent the shielding enclosures and coaxial outer layer. The volume V_2 contains the housings $V_{2,1}$ and $V_{2,2}$, which are volumes representing computer units connected by unshielded communication cable. The symbol $T_{0,2}$

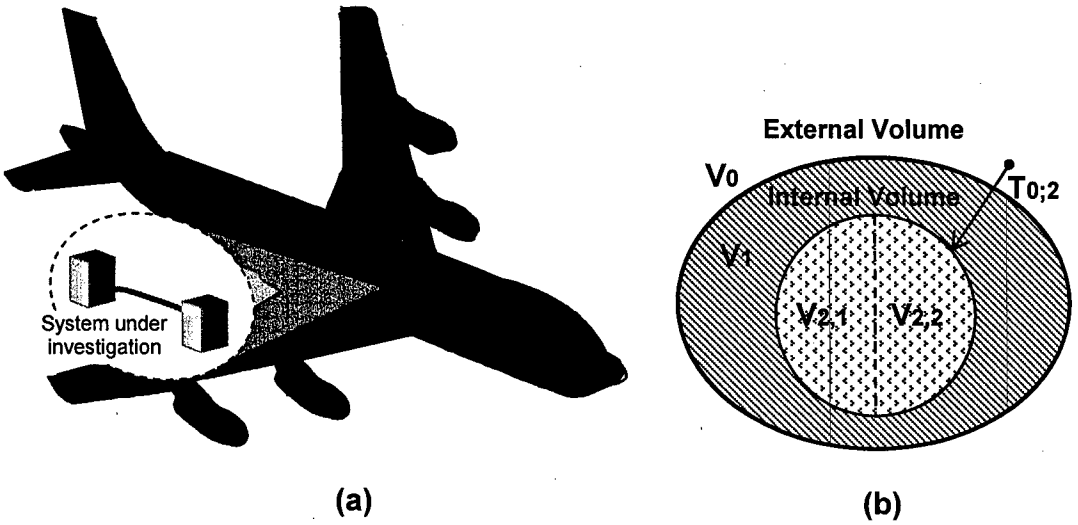

Fig. IIA-1 EMT volume decomposition of a simplified aircraft system.

represents the transfer function from volume V_0 to volume V_2. Two types of transient external excitation sources such as direct-lightning strike and EMP are compared in this study.

External Field Couplings at Volume V_0

Consider a simplified aircraft system with an energy penetration path (aperture). For EMT analysis the interactions of an outside electromagnetic pulse and a wire can be represented as a coupling between an external volume that encloses an internal volume. The coupling parameter is the transfer function that needs to be determined. The primary step is to determine the exterior equivalent sources at the aperture in terms of the surface current and charge densities on the exterior surface by short-circuiting them with perfect conductors, i.e. the conducting surface is made continuous, extending over the region where the aperture existed, as shown in Fig. IIIA-2(a). The equivalent dipoles are placed at the shorted aperture. By imaging the equivalent dipoles p_a and m_a on the opposite side of the

shorted surface, the radiated fields from these dipole moments can be calculated, as shown in Fig. IIIA-2(b).

Thus a short imaginary transmission line, as shown in Fig. IIIA-2(c), can be created with the normalized driving series voltage and transverse current sources that relate respectively to the electric field E_{sc} and magnetic field H_{sc} coupling on the surface as their associate frequency responses caused by the lightning and EMP are shown in Fig. IIIA-3. The aperture then acts as an illumination source for the internal circuitry of the system according to the reciprocity theorem. The CRIPTE topological network of the configuration in Fig. IIIA-2(c) can be shown in Fig. IIIA-2(d)

Transfer Function of Volume $V_0 - V_2$

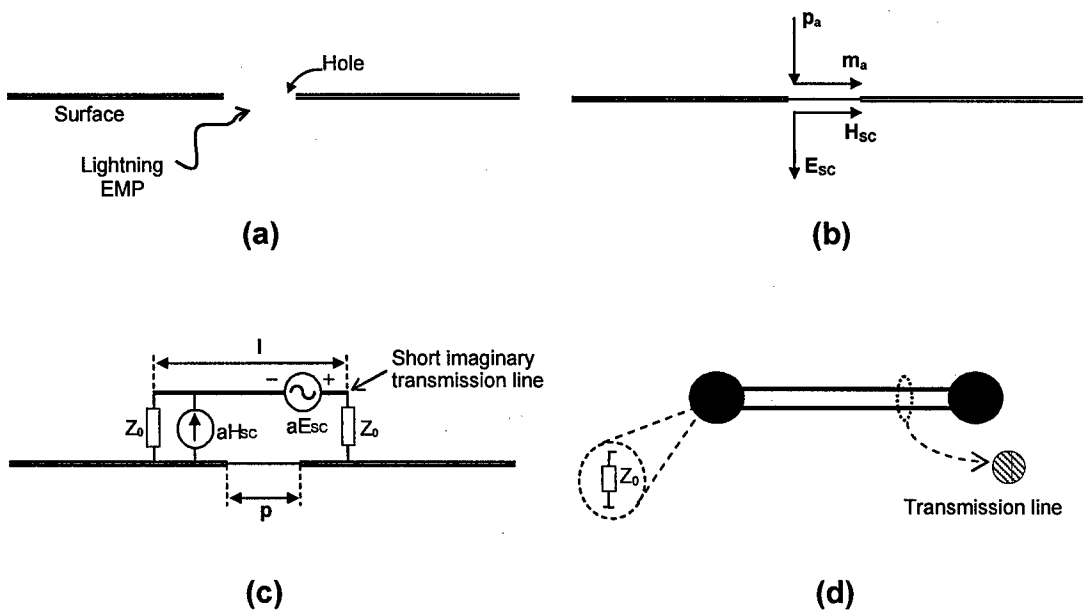

Fig. IIIA-2 Imaginary transmission line representing the field external couplings on the aircraft surface.

The system field penetration is described by the characteristics of the radiated fields caused by the short imaginary radiating dipole method. The radiated or incident electric field E_{inc}

and magnetic field H_{inc}, therefore, excite the transmission cable inducing the voltage and current propagation. The relationship of the sources at the aperture and the fields at the interior cable through the transfer function can be written as

$$(Einc, Hinc) = TF(aEsc, aHsc). \qquad \text{(IIIA-1)}$$

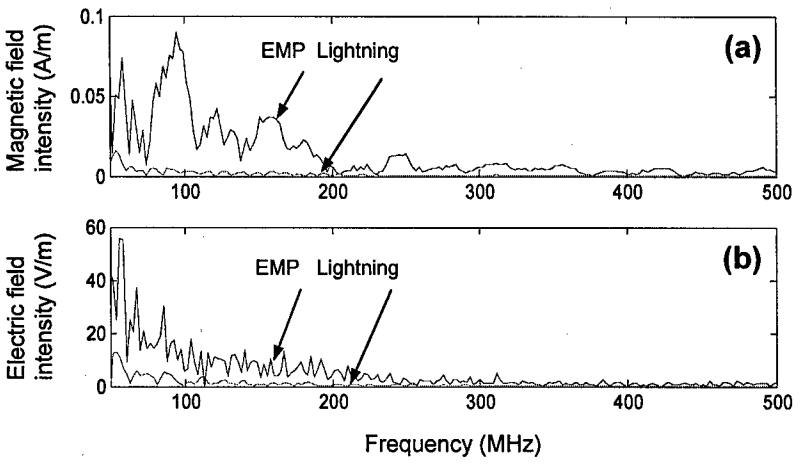

Fig. IIIA-3 Lightning and EMP Fourier spectral waveforms at the aircraft exterior for (a) magnetic fields *Hsc* and (b) electric fields *Esc*.

Fig. IIIA-4 shows the variation in transfer function *TF* in (IIIA-1) with frequency and distance *R* under the lightning excitation. The transfer functions were determined through the relationship of aH_{sc} at the aperture and H_{inc} at 1, 5, 10, and 20 m from the aperture. The relationship shows that near aperture fields have higher values than at a larger distance and frequency dominance is evident as the frequency increases. One would say that the behavior of the transfer function is similar to the high pass filter. The transfer functions so determined are similar to those previously measured through experiments. The same can be said for the transfer function where the definition is determined using E-fields as shown in (IIIA-1).

Cable Excitation inside Volume V_2

The code allows for Taylor or Agrawal's method for the coupling of the radiated waves with the wires. To generate the transfer functions we have used the Taylor formulation since it consists of both current and voltage sources that are appropriate for localized excitations through small apertures and given by

$$V_s(z) = -j\omega\mu_0 \int_0^h [H_y^{inc} + H_y^{ref}]\,dx \qquad \text{(IIIA-2)}$$

$$I_s(z) = -j\omega C \int_0^h [E_x^{inc} + E_x^{ref}]\,dx\ . \qquad \text{(IIIA-3)}$$

To investigate the effect of the EMP and lightning on the system, the current signals on a simple bare wire between two mainframes are observed without and during the excitation. The distance from the aperture, *R*, (see Fig. IIIA-4) is fixed at 5 m. The cable is driven by a 1V-voltage source and terminated at both extremities with various impedances. The CRIPTE topological network for the internal coupling and excitation is shown in Fig. IIIA-5(a) for a bare wire and Fig. IIIA-5(b) for a multi-conductor cable.

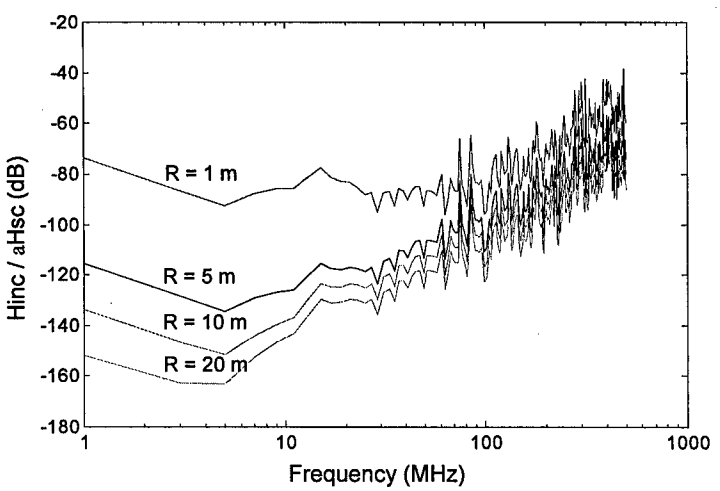

Fig. IIIA-4. Transfer function or the ratio of *Hinc* to *aHsc* in dB as functions of the distance *R* and frequency.

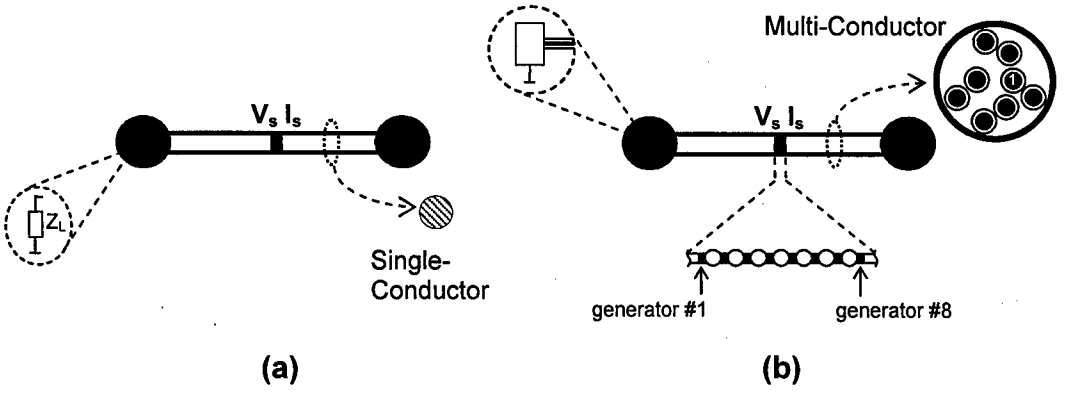

Fig. IIIA-5 CRIPTE configurations for topological network with internal cable: (a) a single-conductor cable and (b) a multi-conductor cable.

Fig. IIIA-6(a) shows the frequency responses of currents observed at the midpoint on a 2-m single-wire cable in the frequency range up to 500 MHz without the excitation when the cable terminations Z_L are matched (mc), open-circuited (OC), short-circuited (SC), 100 Ω, and 1000 Ω as labeled. For mismatched terminations, an increasing number of resonances occur as the frequency increases. The high-frequency resonances on the cable currents depend on the line length and termination impedances of the internal circuitry. The first resonances occur at 75 and 150 MHz for open and short-circuited impedances, respectively. The current responses under the lightning and EMP threats was generated by applying voltage and current generators as localized sources on the cable and is due to excitation from the incident waves. The results for lightning and EMP are shown in Figs. IIIA-6(b) and IIIA-6(c), respectively and can be compared with Fig. IIIA-6(a), which is without the external disturbances. As compared to Fig. IIIA-6(a), Fig. IIIA-6(b) shows that the communication signal between the two units will be perturbed as a result of lightning. The severity of perturbation depends on the value of the terminating impedance. Terminating the cable with high impedances shows that the current signal has major contribution from the *E* field component (related to the current generator) while at low impedance terminations the current signal is influenced mainly by the *H* field component (related to the voltage

generator).

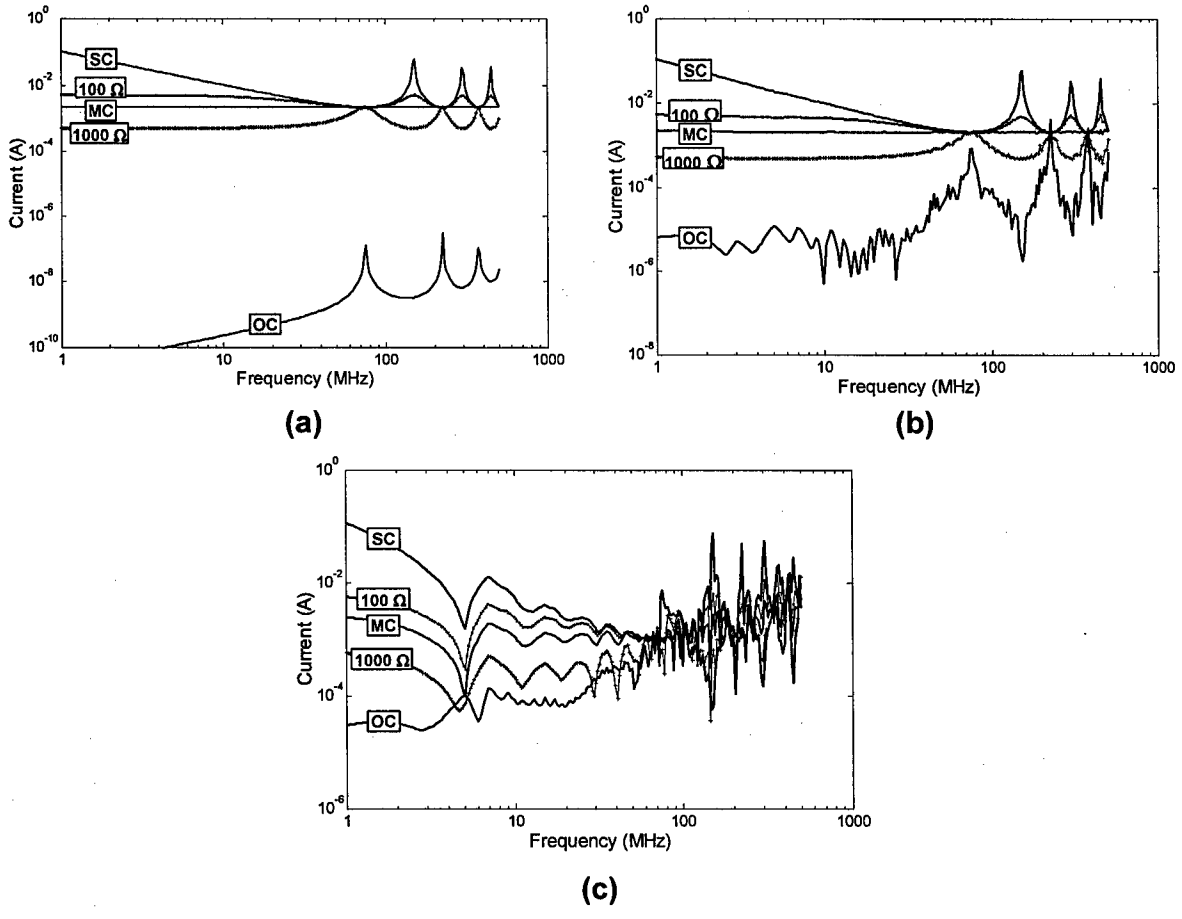

Fig. IIIA-6 Frequency responses of cable currents (a) without and with the excitations of (b) lightning and (c) EMP when the cable terminations are matched (MC), open-circuited (OC), short-circuited (SC), 100 Ω, and 1000 Ω. (— MC, --- OC, ···· SC, -×- 100 Ω, and -+- 1000 Ω).

In Fig. IIIA-6(b), however, only a partial contribution from the lightning-induced H field can be observed on the cable current for the low impedance cases such as short-circuit and 100 Ω since the influence from the H field is relatively low compared to that of the driving voltage source. On the other hand, for the high impedance cases such as open-circuit and 1000 Ω the contributions from the E field dominate. Similar plots of the current responses due to the EMP can be observed in Fig. IIIA-6(c). All cases obviously show the extensive influence of the excitation E and H fields due to EMP on the cable current. The results

caused by both excitations also show that the magnitudes of the currents at high frequencies are much greater than at low frequencies. This result is comparable with experiments where the high frequency field intensity values can be attributed to the resonances and zeros on the cable signals.[3] Therefore, under external electromagnetic perturbations, not only incident electromagnetic waves but also cable resonant characteristics have influences on the current signals.

Interaction on computer network communication

EMT-based simulations of the electromagnetic interaction of the cable network can be implemented through the CRIPTE code by studying the communication between two CCUs shown in Fig. IIIA-7(a). The cable essentially connects the two Ethernet card in each computer. Each Ethernet card (Netgear 10/100 Mbps PCI model FA311) is connected to a computer, which acts as a junction for the CRIPTE code. Measured S-parameters will serve as the input to the junctions of the simulation network. Since the Ethernet card has only one physical port (although it may have two logical ports, one for sending another for receiving) the simulation target is to obtain the S_{11} parameters or the reflection coefficients. The data set of the measured S_{11} parameters is recorded from the network analyzer HP 85047A (300 kHz - 3 GHz) sweeping between 50 and 500 MHz. The measurement is carried out with and without power on the Ethernet card. The data is saved in the ASCII format. The file contains the data of amplitude and phase of S_{11} at 201 frequency points between 50 - 500 MHz. The ASCII file is then imported to the CRIPTE simulation using the ASCII-CRIPTE conversion feature. The output file from the conversion is in the S-matrix format, which is stored in the complex numbers at various frequencies. This file is read-in to the code at the appropriate junctions.

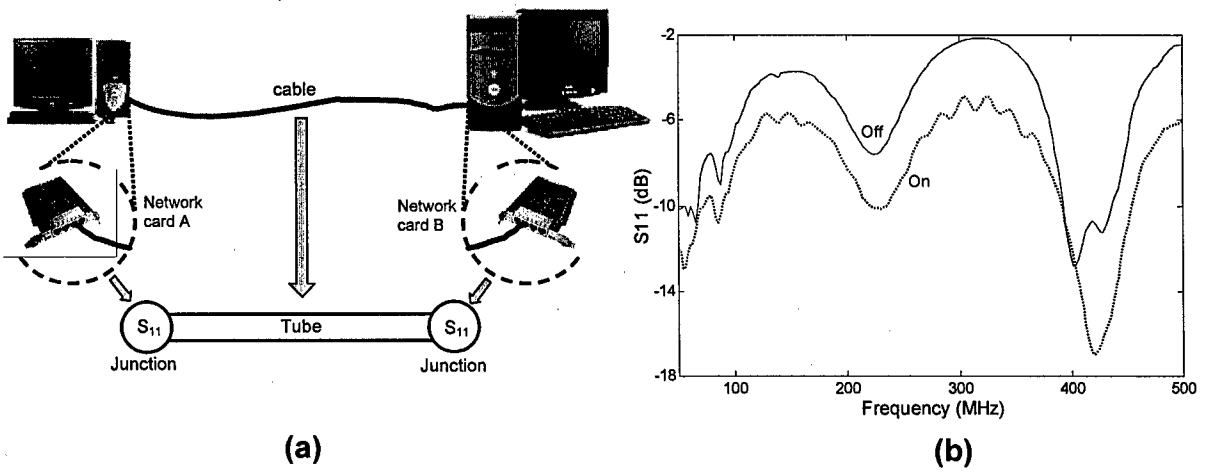

Fig. IIIA-7 (a) Configuration of communication network system with CRIPTE network representation. (b) Measured |S11| parameters (dB) on one port of the network card with and without the supplied power.

The plots of measured $|S_{11}|$ parameters of the network card in dB with and without the power are shown in Fig. IIIA-7(b) as labeled "on" and "off", respectively. The plots show that the least reflections occurred at 420 MHz and 400 Hz for the "on" and "off" cases, respectively. For the simulation study as long as the crosstalk is not our concern, instead of a basic communication multi-conductor cable (UTP CAT-5), the single wire cable with the same conductor dimension was used as to appropriately match with an only available data-sending port on the network card. Shown in Figs. IIIA-8(a) and IIIA-8(b), respectively, show the cable currents as a function of frequency along the cable length without and with the power to the network card. The results show that current due to the external sources are more pronounced at high frequencies and a probable cause for data fault or, communication breakdown. In addition, the simulation results also showed that the impact is more pronounced for the EMP than the direct-lightning strike.

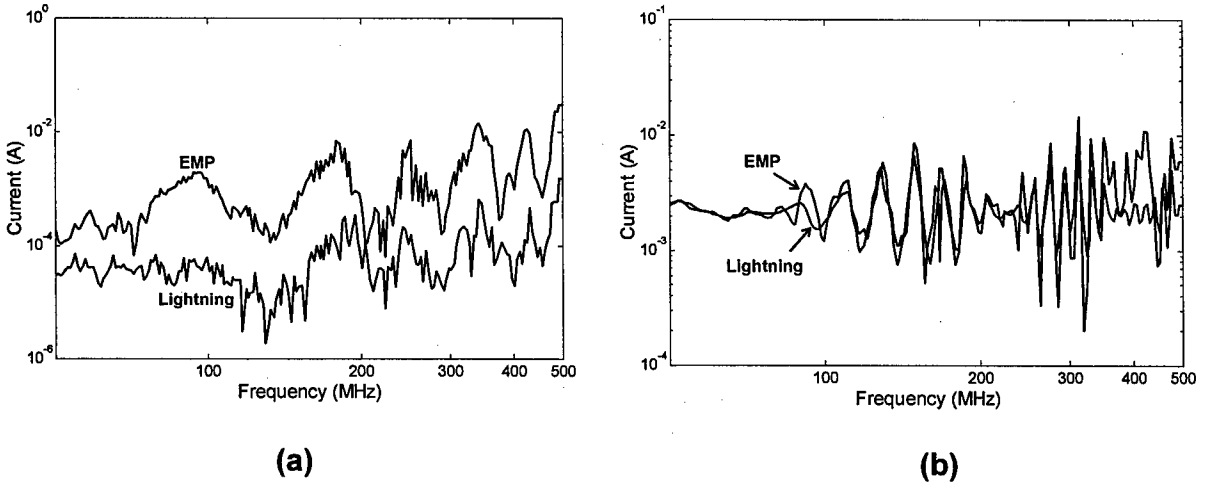

Fig. IIIA-8 (a) Current frequency responses on the cable when the network card is not powered under EMP (solid line) and lightning (dotted line) excitations. (b) Current frequency responses on the cable when the network card is powered under EMP (solid line) and lightning (dotted line) excitations.

Related Publications

A number of technical reports, papers and book article related to this novel application of CRIPTE code in the area of RF interactions were generated ([2006B1], [2005B1], [2005J2], [2005C6], [2005C7], [2004J1], [2004J2], [2004J3], [2004C1], [2004C2], [2004C3], [2004C4], [2004C5]).

(B) Interaction Studies: MTLN and FDTD Analyses for Aperture Interactions

This section shows the application using the Finite-Difference Time-Domain (FDTD) technique on the field couplings on the external surface as a complement to the coupling from the measurements. Consider system shown in Fig. IIIB-1(a), with shielding structures SS_1 and SS_2 protecting electrical systems E_1 and E_2, respectively. E_1 and E_2 are connected to each other by a cable running through an opening O_2. Structure SS_1 also has an aperture O_1 and hence is a semi-shielded system, allowing wave penetration. EMT volume decomposition of Fig. IIIB-1(a) is shown in Fig. IIIB-1(b). Volume V_0 is the proper volume covering the entire system. Volumes $V_{1,1}$ and $V_{1,2}$ are the elementary volumes representing structures SS_1 and SS_2 respectively. The volumes $V_{2,1}$ - $V_{2,4}$ are the elementary volumes for electrical systems

and the connecting cables. The first shielding level $S_{0;1}$ (structure outer surface) and the second shielding level $S_{1;2}$ (surfaces of cable outer layer and electrical system housings) separate the volume V_0 and $V_{1,n}$, and $V_{1,n}$ and $V_{2,n}$, respectively.

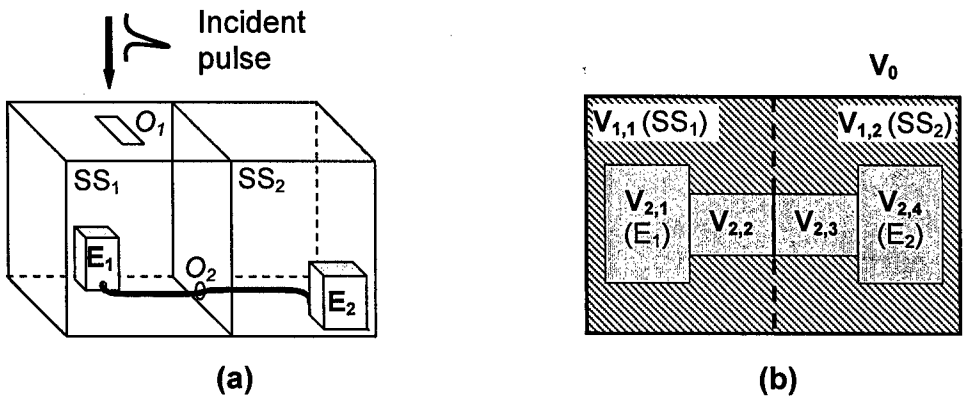

Fig. IIIB-1 Diagrams of (a) the shielded rooms with aperture and (b) the volume decomposition.

The system coupling using the short imaginary radiating dipole method is shown in Fig. IIIB-2 as represented by network I. Network II in Fig. IIIB-2 represents components and connections of the system interior. It consists of two main tubes (T_1 and T_2) for eight-conductor cables and two junctions (E_1 and E_2) for the terminating impedances of both electrical modules and one junction (O_2) for the straight-through connection type between cables T_1 and T_2. The dotted-line junction between E_1 and O_2 represents the coupling on tube T_1 of the distributed equivalent generator V_s originally generated by the topological network I.

The equivalent voltage generators, which represent distributed source couplings on the cable over the ground plane, are derived from the incident electric field on the cable and from the reflected electric field from the ground plane in the absence of wiring so as to avoid wave reflection. The coupling methods of the incident fields on the cable incorporated in the code can be implemented through the Agrawal's formulation,[4] as given by

$$V_s(z) = E_z^{inc}(h,z) + E_z^{ref}(h,z). \quad \text{(IIIB-2)}$$

By incorporating the voltage in (IIIB-2), the source waves in (IIIB-1) can be written as

$$[Ws(z)] = \int_0^z \left[e^{-\gamma(z-z')}[V_s(z')] + [Z_C][I_s(z')]\right]dz', \quad \text{(IIIB-3)}$$

where [γ] is a propagation matrix and $I_s(z) = 0$ for the distributed source coupling. Then the voltage and current along the transmission line in the z direction can be determined through the definition of waves by

$$[W(z)] = [V(z)] + [Z_C][I(z)]. \quad \text{(IIIB-4)}$$

In both the FDTD and EMT simulation approaches, we consider the case when the dimension of the aperture is electrically small relative to the wavelength. The results were first simulated using the FDTD method based on Yee's algorithm in free space.[5] The cell dimension is much less than the minimum wavelength. The finite difference equations in three dimensions have the same spatial steps as $\Delta x = \Delta y = \Delta z = 6$ mm. Once the grid size was defined, the next consideration was the stability by choosing the small enough time step Δt. The appropriate choice is $\Delta x/2.c$ which gives 10 ps where c is the speed of wave in free space. An incident Gaussian pulse is applied as the y-polarized excitation of the difference equations given by

$$E_{inc} = E_0 e^{[-(n\Delta t - t_0)^2/2\sigma^2]}, \quad \text{(IIIB-5)}$$

where E_0 is the peak amplitude, t_0 is the original location of the peak, and σ is proportional to the pulse width. Fig. IIIB-3 shows the FDTD generated *H*-field (Hsc) and the *E*-field (Esc) waveforms at the screen when the aperture is short-circuited when E_0 is unity. The waveforms in Figs. IIIB-3(a) and IIIB-3(b) are Hsc and Esc, respectively, for the 3.6-ns incident Gaussian pulse. Figs. IIIB-3(c) and IIIB-3(d) are the corresponding Hsc and Esc, for the 0.36-ns incident Gaussian pulse. These waveforms are used in the radiation dipole

antenna to generate fields at a distance from the aperture.

To examine the effect of the electromagnetic fields on the system interior, the voltage signals propagating between both computers (E_1 and E_2) were simulated. The excitation sources are incident Gaussian pulses as the mechanism of the penetration through the aperture was previously discussed. The 1-m multi-conductor cable connecting both terminals is driven by a 1-V driving voltage source applied at the terminal E_1 on conductor #1, as labeled in Fig. IIIB-2. The terminating impedance of each port was represented by a 50-Ω resistance.

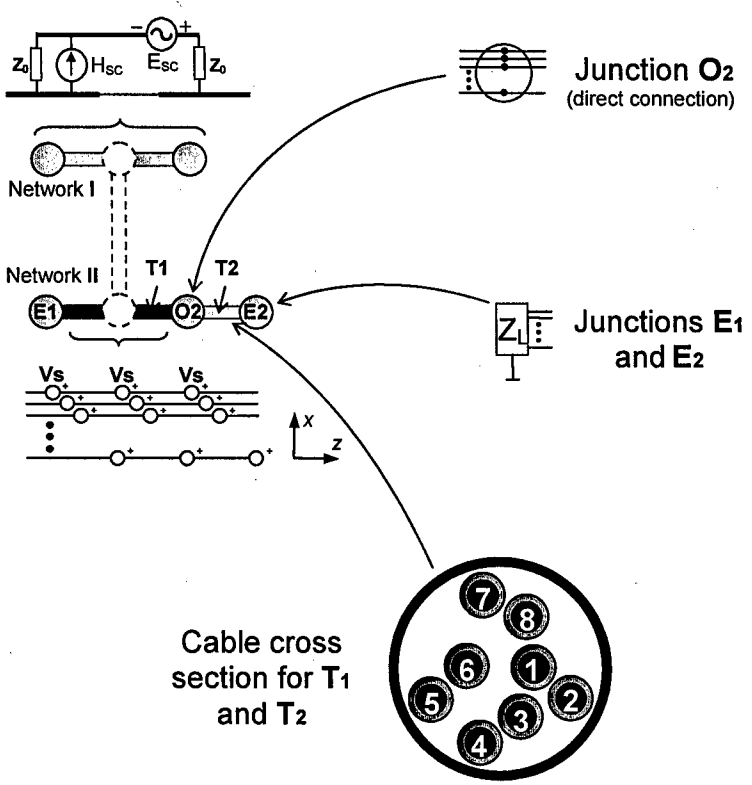

Fig. IIIB-2 Detailed configuration of topological networks and their components used in the EMT calculations.

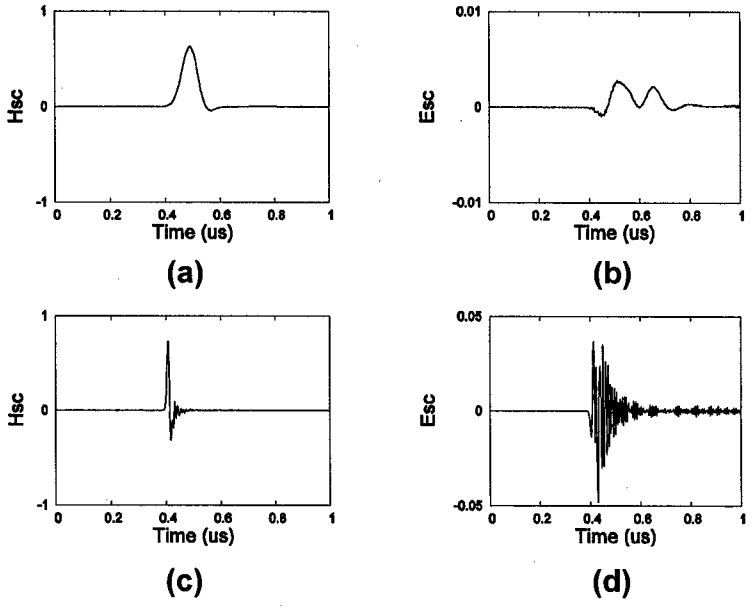

Fig. IIIB-3 Time-domain plots of (a) H_{SC} and (b) E_{SC} due to a 3.6-ns Gaussian incident pulse, and (c) H_{SC} and (d) E_{SC} due to a 0.36-ns Gaussian incident pulse.

The simulation results show the behavior of the signals before and after being disturbed by external excitations. Figs. IIIB-4(a) and IIIB-4(b) show the spectral components of the cable voltages at E_1 and E_2, respectively, for each conductor (#1 through #8) without any influence caused by external perturbations. The strongest signal appears on conductor #1 as it is driven by the voltage source. The responses on the other conductors are the crosstalk signals induced by the signal on conductor #1. The associated voltage responses of the system after being excited by the Gaussian pulses are shown in Figs. IIIB-4(c) through IIIB-4(f). The results shown in Figs. IIIB-4(c) and IIIB-4(d) for the cable signals at terminal E_1 and E_2, respectively, show that the 3.6-ns incident pulse at the outer surface can upset the cable signals when the disturbing frequency range is from dc to 10 MHz. For the system under the external excitation caused by the 0.36-ns incident pulse, the upset zone can be observed at frequencies from approximately 100 MHz to 200 MHz, as shown in Figs. IIIB-4(e) and IIIB-4(f) for terminals E_1 and E_2, respectively. The reason is that the amplitudes of pulse spectral

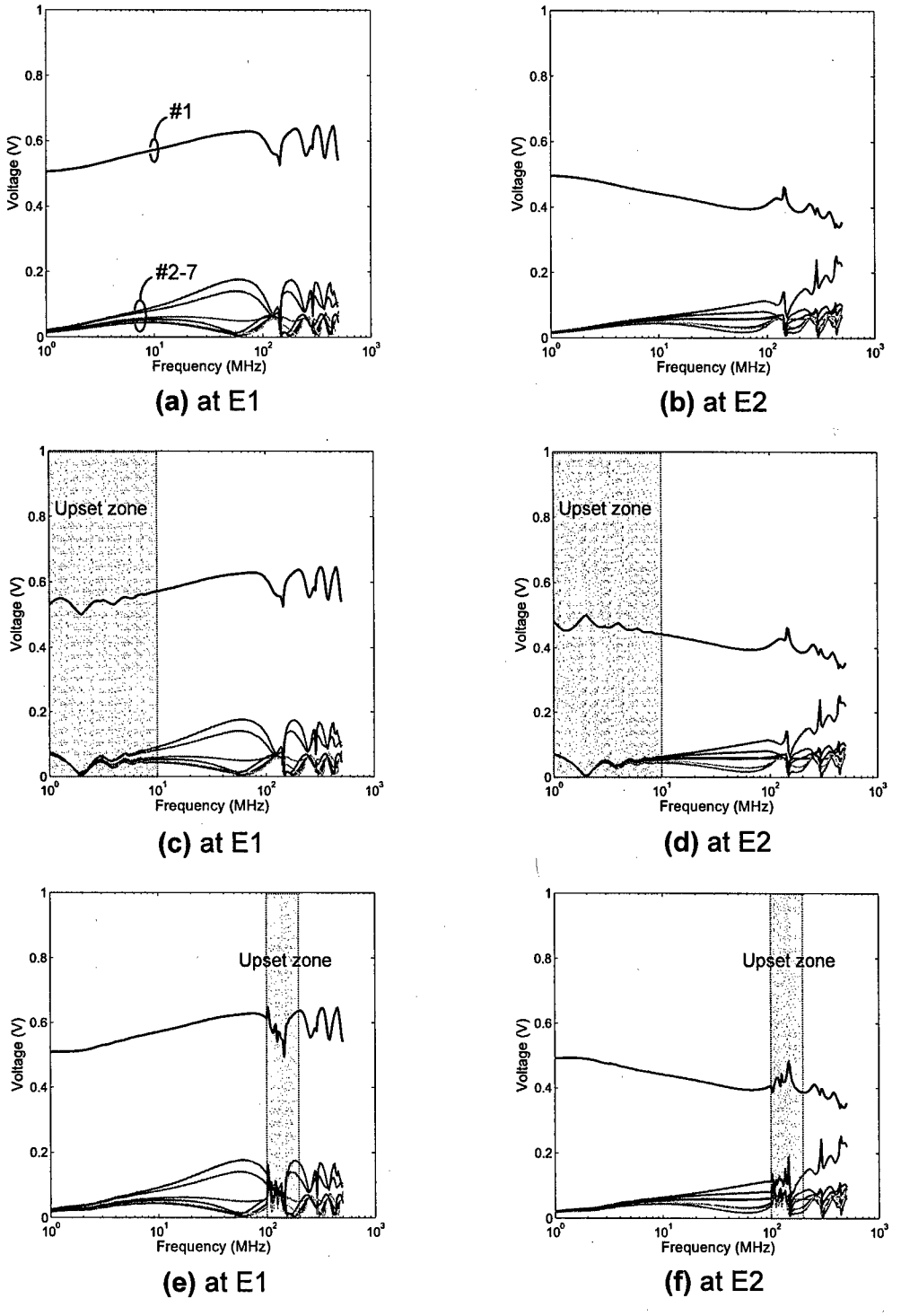

Fig. IIIB-4 Voltage spectral components of individual conductor at both terminals: (a)-(b) without excitation sources, (c)-(d) with a 3.6-ns Gaussian pulse, and (e)-(f) with a 0.36-ns Gaussian pulse. (E_0 = 1e3).

contents account for the behaviors of the cable responses. The 3.6-ns Gaussian pulse has large-amplitude frequency components at low frequencies while those of the 0.36-ns Gaussian pulse exist at high frequencies.

Severity of the effects at high frequencies is of concern since the faster rise time of external perturbations induced the voltage to increase in amplitude. In addition, the cable resonances due to the mismatched impedances at cable extremities have a tendency to magnify the signal propagating on the cable as the frequency increases. Finally the results also show that even though the sensitive electrical system, i.e. E_2, is securely protected by the shielded wall, the disturbance can still be introduced into the system by the cable interaction through the wall.

Related Publications

Related works to this interaction study are reported in the book article [2005B1], paper [2005J3], and technical report [2005C6].

(C) Interaction Studies: MTLN-TLM Analysis for Quasi Aperture Interactions

In this study we propose an alternate approach to simulate external EMP and aperture interactions. It may be described as a two step process. First there is an initial process of interaction that results in scattering fields at the aperture. These fields then propagate to the other side where further interactions may occur. The schematic of such an approach is shown in Fig. IIIC-1. Here the EM wave interacts with a system primarily through the fields generated at the aperture in an infinite metallic plane, as shown. We concentrate primarily in generating the aperture fields and verify the results by comparing it with a FDTD code. In short, we propose a simpler and accurate methodology, which combines the EMT approach with the transmission line matrix (TLM) method to account for the coupling of an incident electromagnetic field with an aperture over an infinite metallic plane in a topological

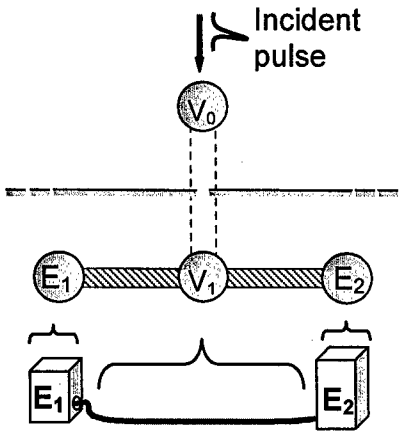

Fig. IIIC-1 Configuration of a semi-shielded system and topological network treating the system interaction mechanism with a 2D aperture.

simulation setting. It does not require experimental field values for aperture radiation as was needed in our previous work.[6] Finally, we also describe a method for applying compaction techniques that result in a more efficient computation without sacrificing accuracy.

Aperture in Electromagnetic Topology

The electromagnetic topology simulation concept and methods is not the subject of study here. In short, topological simulations for a given electrical system require a volume decomposition of the geometry and the creation of a circuit for simulations. For topological breakdown into volumes and then into junctions and tubes for interaction problems, consider Fig. IIIC-1. The figure shows a system with two semi-shielded, electronic devices, E_1 and E_2, connected to each other by an unshielded cable. The topological network for such a system is shown immediately above it as two circular devices connected by a tube-like structure. At the junction of E_2, vectors for both the incoming ($W_1(L)$) and outgoing waves ($W_2(0)$) are related by the junction scattering matrix (S_{12}) through the scattering equation, expressed as

$$(W_2(0)) = (S_{12})(W_1(L)). \qquad \text{(IIIC-1)}$$

For multi-conductor lines, the incoming and outgoing waves at the junction of E_2 can be represented, respectively, by $(V)+(Z_c)(I)$ and $(V)-(Z_c)(I)$ where (V) and (I) are voltages and currents at each port of the junction and Z_c is the characteristic impedance. The scattering parameter (S) can be written in terms of the admittance matrix (Y) as in equation (IIIC-2), with the characteristic impedance matrix at the junction of E_2 with $N1$ conductors along tubes is represented through equation (IIIC-3):

$$(S) = [(1) - (Z_c)(Y)][(1) + (Z_c)(Y)]^{-1}, \tag{IIIC-2}$$

$$(Z_c) = \begin{pmatrix} Z_{c1,1} & \cdots & Z_{c1,N1} \\ \vdots & \ddots & \vdots \\ Z_{cN1,1} & \cdots & Z_{cN1,N1} \end{pmatrix}. \tag{IIIC-3}$$

Propagation of the incoming and outgoing waves, along the tube in the opposite directions with an equivalent distributed source (Ws), can be characterized by a propagation matrix (Γ). The resulting propagation equation becomes

$$(W_1(L)) = (\Gamma)(W_1(0)) + (Ws). \tag{IIIC-4}$$

Signals on an entire transmission-line network is expressed through the BLT (Baum Liu and Tesche) equation which is in essence, the multi-conductor transmission line (MTL) network composed of the incoming wave vector, the outgoing wave vector, and the source wave super vector, respectively, shown above as $[W(0)]$, $[W(L)]$, and $[Ws]$ as detailed in reference.[2] The network scattering and propagation super matrices are represented, respectively, by $[S]$ and $[\Gamma]$. Using the supervector and supermatrix forms seen in (1) and (4), the BLT equation can be expressed as

$$\{[I] - [S][\Gamma]\}[W(0)] = [S][Ws], \tag{IIIC-5}$$

where $[I]$ is the identity super matrix. Solutions of the BLT equations have been incorporated into an electromagnetic topological code that uses the LU decomposition method.

We designate V_0 as the volume covering the entire system, V_1 as volume underneath

the aperture plane, and E_1 and E_2 as the volumes housing the electronic devices. The objective of this work is to device a mechanism to integrate a TLM method with the MTLN formulation for EMT solutions that describes only the interactions of the external pulse with the aperture. The consequent propagation process described earlier is not attempted here. That is, the cable coupling (a coupling mechanism of junction V_1 and internal horizontal tube) in the internal volume is left for future work. The topological network for the aperture penetration, thus, consists of junctions, V_0 and V_1 with the dotted line tube signifying the interaction between these two volumes.

Interactions with the aperture can be best described through the TLM method. This is because the TLM method is a physical discretization of a field where a continuous system is replaced by a network of lumped elements. Due to equivalence between Maxwell's wave propagation equations and transmission-line equations, one would appropriately relate the electric and magnetic fields with voltages and currents on the transmission lines. With suitable boundary conditions, aperture interaction problems can be solved by the TLM method and integrated into the topological solution as described in the following section.

Integration Transmission Line Matrix with EMT Compaction Solutions

The TLM solution approach has been extensively used in many EM-related applications both in time and frequency domain.[7,8] The time domain technique best suits simulating wave propagation in guided wave structures with arbitrary shapes and uses a band limited pulse excitation for studying frequency ranges. Thus for full impulse response, the simulations take a long time before steady state is reached, specifically for large network matrix. In this analysis we chose the frequency domain method because the topological network code works in the same domain. Also, for a uniform cross section a two-dimensional (2-D) solution would suffice.[9] For two-dimensional wave propagation on a transmission line with a shunt node shown in Fig. IIIC-2(a), one can easily solve for Maxwell's equations to get

the current and voltage wave equations with R', L', G', and C' as the per unit length transmission-line parameters,[10]

$$\frac{\partial^2 V_y}{\partial x^2}+\frac{\partial^2 V_y}{\partial z^2}=(R'+j\omega\sqrt{2}L)(G'+j\omega\sqrt{2}C)V_y=\gamma_{tlm}^2 V_y, \qquad \text{(IIIC-6)}$$

And by assuming a lossless line, the above Helmholtz wave equation reduces to

$$\frac{\partial^2 V_y}{\partial x^2}+\frac{\partial^2 V_y}{\partial z^2}=(j\omega\sqrt{2}C')(j\omega\sqrt{2}L')V_y=\gamma_{tlm}^2 V_y, \qquad \text{(IIIC-7)}$$

where γ_{tlm} is the propagation constant of the voltage and current on the TLM network. One can easily obtain the solutions for the TM-mode (TLM shunt node) wave propagation in the homogeneous medium using the correspondent TLM solutions with the parameters as follows:

$$E_y \equiv V_y,\ H_x \equiv -I_z,\ H_z \equiv I_x,\ \mu_0 \equiv \sqrt{2}L',\ and\ \epsilon_0 \equiv \sqrt{2}C' \qquad \text{(IIIC-8)}$$

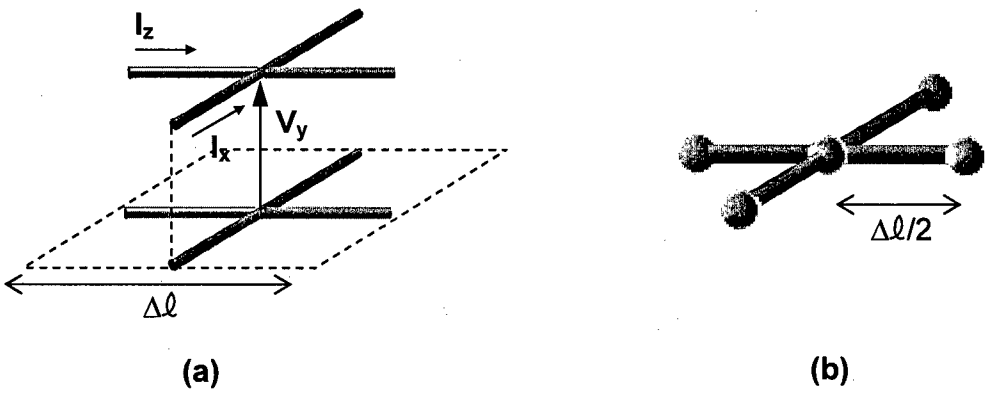

Fig. IIIC-2 (a) TLM equivalent for a shunt node and (b) Topological node representing the TLM mesh node.

This shows the slow-wave property of the 2-D TLM network where the propagation speed in the TLM network is less than the speed of light by a factor of 0.707.[11]

Since the multi-conductor transmission line network is used as the application

domain, an electromagnetic topology-based numerical code can also be used to implement a TLM mechanism in obtaining the wave propagation solutions. Basically, each tube is composed of several small segments of lumped circuit components. As the tube section becomes relatively small ($L = dz = \Delta\ell/2$), one would utilize the configuration of the topological network in Fig. IIIC-2(b) to carry out the TLM solutions. Thus the proposed array of topological matrices, which is based on the TLM network concept, can be used as a complement to a topological technique in order to assess the interactions through medium by modeling all the tubes in the topological code with the line parameters expressed in (IIIC-8).

The network array is characterized by a large number of unknowns, thus resulting in a big spread network system. However, it is possible to break down the spread network into sub-networks, and characterize independently for final cascade integration. This segmentation is based on the diakoptics technique which is suitable for the repeated analysis

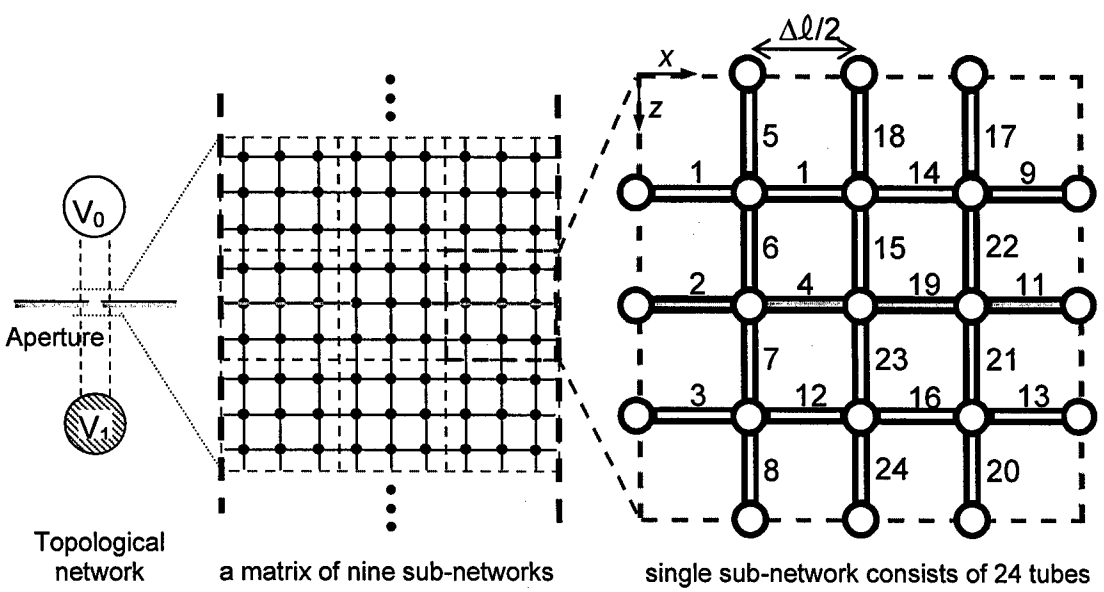

Fig. IIIC-3 An arrangement of tube-junction network for a field penetration through an aperture.

of large networks where only a small part is different from others.[12] In our simulations, we consider only a single part of the topological network, which is, in fact, an integration of nine sub-networks. In the same arrangement as the TLM network, each sub-network is created from 24 tubes labeled as shown in Fig. IIIC-3. An equivalent junction is then created through compaction.

Since the entire cable network comprises a large number of junctions and tubes, direct calculation using the BLT equations is very cumbersome and time consuming. The compaction method allows for a modular solution to the network problems. It allows for the solution of a subset of the spread network and then integrating all subsets into one final solution. By letting this modular concept of creating the equivalent junction, the calculation no longer has to re-compute all subsets of a large network. This equivalent module so created can also be used in other topological networks.[13] Fig. IIIC-4(a) shows the configuration of the compaction on the sub-network seen in Fig. IIIC-3. The black nodes are defined as the internal junctions located inside the dotted-circle. The internal junctions are related together by the internal tubes. The external tubes characterize the relationship between the internal junctions and the external (terminal) junctions, which characterize the open circuits as represented by the white nodes. This figure also shows a twelve-port, four-directional equivalent junction (con4.seq) as a result of the compaction of the associated sub-network seen in Fig. IIIC-3. The number of external nodes of the sub-network corresponds to the number of output ports of the equivalent junction. In fact, the equivalent junction only characterizes the scattering inside the sub-network independent of the applied source. Therefore, the junction is the matrix characterized by the individual S matrix of internal junctions and the Γ matrix of internal and external tubes.[13] Also shown are the two and three-directional equivalent junctions (con2.seq and con3.seq).

The equivalent junctions under incident plane wave excitation (*Ws*) are created with

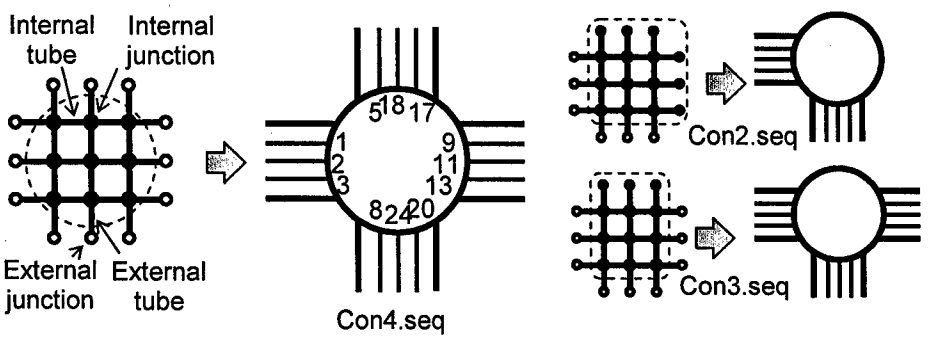

(a)

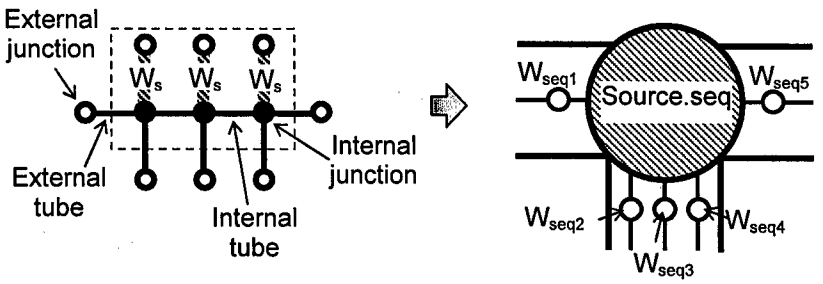

(b)

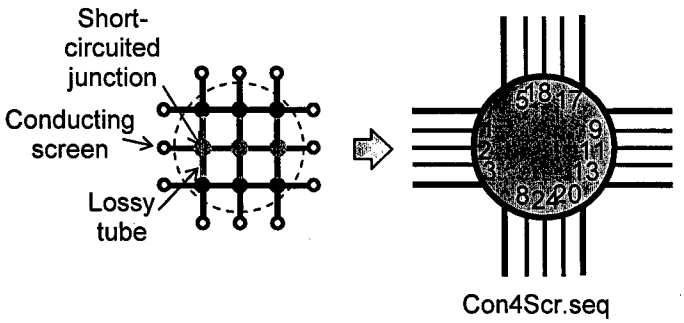

(c)

Fig. IIIC-4 Compaction on the sub-network in Fig. IIIC-3: (a) regular equivalent junctions, (b) equivalent junction with internal sources, and (c) equivalent junction with metallic conducting screen.

the addition of Thevenin equivalent generators. The concept is to create the vectors *Wseq* that define the equivalent sources located at the terminals of the equivalent junction. By applying *Ws* on the internal tubes with the external terminals opened, the resulting *Wseq* are equal the open circuit voltage induced on the output ports. The corresponding algorithms are illustrated in Fig. IIIC-4(b). The equivalent junctions representing the conducting screen must satisfy the boundary conditions on the tangential and normal components of the fields.[14] The tangential component of the electric field disappears as does the corresponding normal components to the screen of the magnetic field. The modeling of the equivalent junction is described in Fig. IIIC-4(c) with short-circuited internal junctions and associated tubes with high resistances. The equivalent-junction network for this study consists of a regular junctions, plane-wave-source junctions, and screen-with-aperture junctions as shown in Fig. IIIC-5(a). The tubes connecting two equivalent junctions have the length of zero because their actual dimensions have already been defined through the external tubes (Fig. IIIC-4) during the compaction stage.

For simulations without compactions, the matrix size required for each sub-network is 96 (4 × 1 × 24), i.e. 4-directional junction, 1-conductor wire, and 24 tubes. With compactions (Fig. IIIC-4(a)), the original matrix reduces by half to 4 × 3 × 4 = 48. We compute the matrix numerically just once and cascade this equivalent junction to others network arrays. The number of junctions required for the compacted network is 9 when the source junctions are not taken into account. Original network without compaction require 81 junctions.

With this configuration, it is possible to continue with simulations for penetration through the aperture in free space by the topological network. Also the size reduction of the network shown in Fig. IIIC-3 can improve the speed of calculation as well as the memory requirement. The simulations focus on the field propagation through the aperture located at

the boundary between the outer volume (V_0) and the volume underneath the aperture plane (V_1).

Both the FDTD and topological simulations are carried out on a Pentium XEON-processor Linux server. Results from topological simulations and finite difference time domain (FDTD) technique,[5] were compared using a Gaussian electromagnetic pulse that penetrates through the sub-wavelength aperture. All FDTD cell dimensions used in the network have the same spatial steps of 6 mm, which is much less than the wavelength associated with the central frequency of an incident Gaussian pulse. The incident pulse transmitted through the aperture has a 3.6-ns Gaussian pulse width and is excited for y-polarization, given by

$$E_{inc} = E_0 e^{[-(n\Delta t - t_0)^2/2\sigma^2]}, \qquad \text{(IIIC-9)}$$

where E_0 is the peak amplitude, $n\Delta t$ is the time increment in step, t_0 is the original location of the peak, and σ is the Gaussian pulse width.

The effects of the aperture width on the transmitted Gaussian pulse through the aperture are shown in Fig. IIIC-5(b). The solid lines in Fig. IIIC-5(b) are the frequency spectra from 50 MHz to 1.0 GHz, which are obtained by a Fourier transform on the FDTD generated E-field waveforms in the time-domain for the aperture widths d at 6 mm (case A), 12 mm (case B), 24 mm (case C), 36 mm (case D), respectively. Fig. IIIC-5(b) also shows the results based on topological simulations. The topological network used has nine sub-network components. The results show that energy coupled into the aperture decreases as the aperture dimension is decreased in accordance with the well known d^3 law whenever the wavelength is much smaller than the aperture width ($\lambda >> d$).[15] The results also show that the amplitudes of the higher spectral components are less distorted as the aperture width increased. It is consistent with the analysis that the small aperture can be approximated using an undersized waveguide model with the very small thickness.[16] Therefore, in the

frequency range smaller than the cutoff frequency, no waves can propagate through the aperture because of the inherent high-pass filtering properties. Incrementing the aperture size also results in the cutoff frequency to shift lower, allowing more penetration of the high frequency components.

In Fig. IIIC-5(b), frequency spectra above the cutoff frequency of case D propagate through the aperture without significant distortion in amplitude while the lower frequency spectra experience frequency dependent attenuation. As the aperture size decreases from case D to case A, more components of the incident Gaussian pulse fall into below the cutoff frequency regions. The spectral components will experience stronger suppression and become flatter, increasing the bandwidth. As a result, the fields transmitted through the aperture will be lower in amplitude caused by suppression and faster oscillation due to the larger relative weight of the high frequency spectral components than the incident pulse.

The calculation speed depends mainly on the resolution of the space step for time domain and the size of the compaction network for topological network domain. Simulations show that the ratio of the total elapsed time used for the FDTD and the topological calculations is 5.6, which is a huge advantage of using the compaction technique with the topological network. For FDTD code, a single calculation step is equal to a half distance of the cell dimension. One, therefore, requires 20000 time steps to achieve the result with corresponding first frequency of 10 MHz while the topological calculation needs 100 frequency steps from the fundamental to final frequency of 1000 MHz. The topological code has an advantage over the time domain code for this particular network size and it can be not true for more complicated arrangements. A validation of the time domain transmitted field for the 6mm case is shown in Fig IIIC-5(a). Since TLM methods are applicable to low frequency, one can see slight discrepancy in the results as high frequency is approached. In addition, the delay of the wave from the EMT code reflects the property of the slow-wave

propagation caused by the use of the shunt node-like configuration.

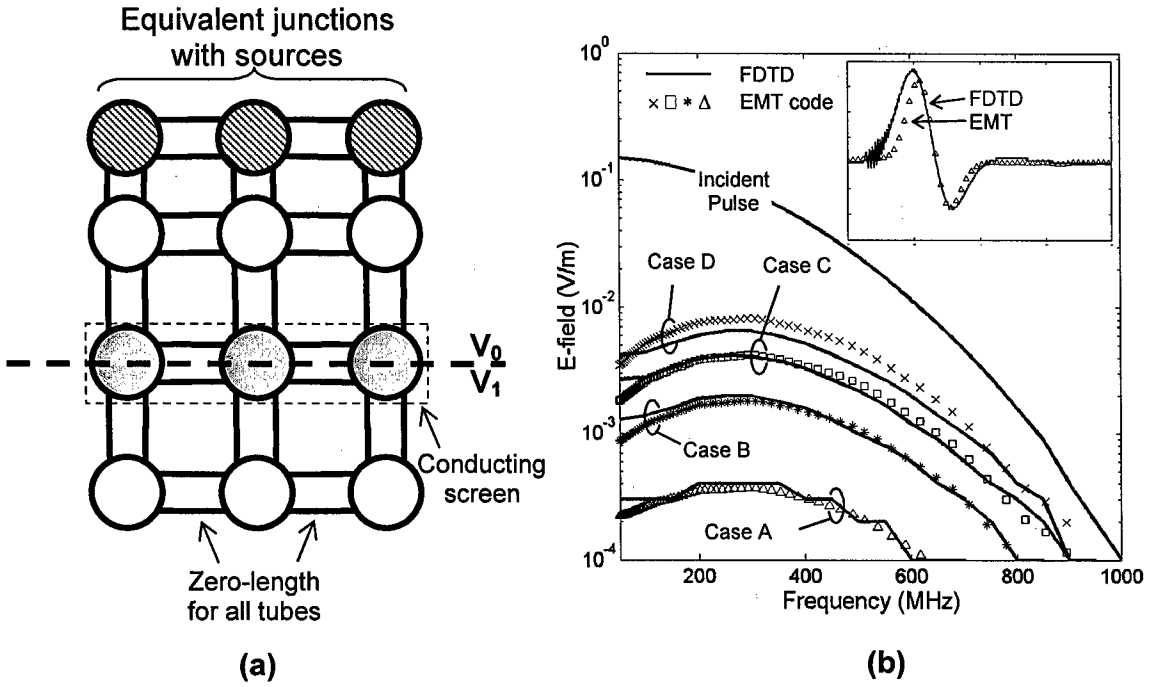

Fig. IIIC-5 (a) Equivalent-junction network used in simulations. (b) Frequency spectral contents of the field transmitted through the conducting screen as a function of the aperture width (case A: 6 mm, case B: 12 mm, case C: 24 mm, and case D: 36 mm) from the FDTD calculations (solid lines) and the EMT-TLM calculations (various markers). Inset compares time-domain transmitted fields for the 6 mm case of both FDTD and EMT calculations.

Related Publications

Related works to this interaction study are reported in the paper [2006J3], and technical reports [2005C1], [2005C2], [2005C3], [2005C5].

(D) Interaction Studies: MTLN Analysis for Cable Crosstalks

In this work we present an alternate simulation approach known as electromagnetic topology (EMT) simulation technique to study crosstalk induced in four pairs of UTP-CAT5 cables for frequency range up to a few hundreds MHz. Simulation is based on a lumped-circuit transmission-line model similar to the configuration used in the work of *Paul and McKnight* [17,18] where it consists of a single-wire generator, two-wire receptor circuit in a homogenous media. The wire separation and length are sufficiently small as to ensure a validity of a low-frequency model. The electromagnetic topology technique is a modular simulation method, specifically suited for electrical systems that are large and can be analyzed through volume decomposition.[13] Details and advantages of this technique, proposed by the Air Force Research Laboratory (AFRL), NM, in the early 1980s, have been reported elsewhere.[1] The main advantage of this technique is to overcome some of the

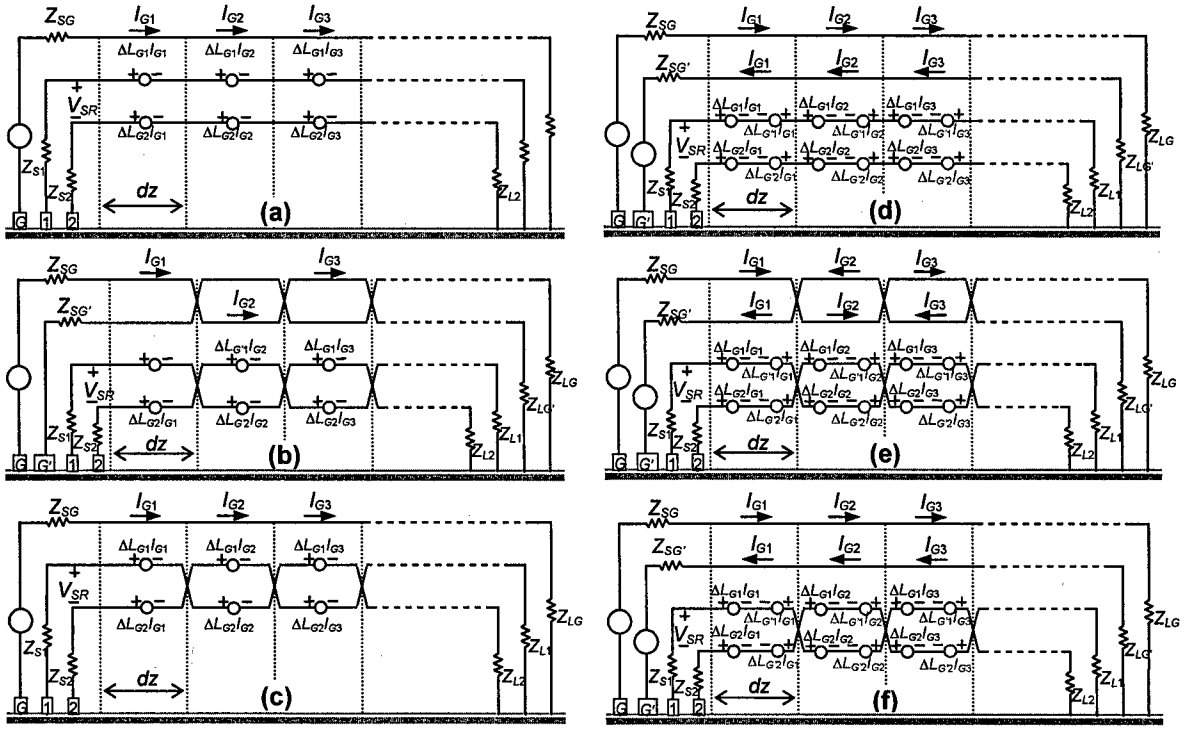

Fig. IIID-1 Coupling models driven by single source of configurations (a) STS/STP, (b) TWP/TWP and (c) STS/TWP, and coupling models driven by differential source of configurations (d) STD/STP, (e) TWPD/TWP and (f) STD/TWP. $\Delta = jwL$.

simulation problems associated with large network systems. In an EMT simulation approach a very large network can be analyzed through volume decomposition. Each volume has different shielding levels and the interactions between the volumes are only possible through cables linking the two volumes or through openings and apertures between them. In this paper we propose a concept for electromagnetic topology simulations to account for the crosstalk caused by the signal propagation through connecting cables using the EMT based code.[19] The key equation of EMT to express the signals on an entire transmission-line network is the BLT (Baum Liu and Tesche) equation.[20]

In the simulation setup we incorporate the multiconductor transmission-line model with various types of generator, receptor, and impedance arrangements in order to analyzed and compared effective crosstalk suppression on 100/1000Base-T networks. The outcome and advantage of such a simulation approach, besides the validation of topological simulation method, is a topological cross-talk suppressed circuit that can be integrated with a larger network for analysis.

Crosstalk Circuit Models

Near End Crosstalk (NEXT) is a coupled interference signal between adjacent cables at the nearest end of the source. It does not depend on the generator and receptor cable length. The NEXT value (in decibels) is computed as the difference in amplitude between the test signal and the crosstalk signal, given by

$$NEXT = 20\log_{10}\left|\frac{V_{SR}}{V_{SG}}\right|, \qquad \text{(IIID-1)}$$

where V_{SR} and V_{SG} are the voltages across the receptor and generator wires at the sending end, respectively. Higher negative values correspond to less crosstalk and better cable performance. By its nature, it will get worse as the frequency increases. In terms of

interference the higher the frequency, the higher the noise coupling on the receptor or the smaller the electrical insulation between the interfering generator and the receptor.

Fig. IIID-1 shows the coupling scheme that has been adapted for the analysis of the configuration shown in Fig. IIID-2(c). The circuits shown in Figs. IIID-1(a) to 1(c) represent single-wire generator, two-wire receptor circuits where they can be subcategorized by a presence of twisted sections, i.e. straight-through single-generator, straight-through receptor (STS/STP); twisted-pair single-generator, twisted-pair receptor (TWP/TWP); and straight-through single-generator, twisted-pair receptor (STS/TWP). The STS/STP model, as shown in Fig. IIID-1(a), is the simplest configuration, i.e. only single wire for the generator (G) and untwisted receptor pair (1-2). Based on the low-frequency approximation, it may assume that the voltages and currents of each section are approximately identical.[18] The differential voltage between receptor wires at the sending end is then given by

$$V_{SR} = \left[\frac{Z_{SR}}{Z_{SR} + Z_{LR}}\right] j\omega dz (L_{G1} - L_{G2})(I_{G1} + I_{G2} + I_{G3} + \ldots), \qquad \text{(IIID-2)}$$

where Z_{SR} and Z_{LR} are source and load impedances, respectively, L_{G1} and L_{G2} are the mutual inductances between the generator and receptor wires, and I_{Gn} is the generator current associated with the nth dz-long wire segment.

Fig. IIID-1(b) shows the TWP/TWP model which is the most common configuration for the UTP-CAT5 cable where both generator and receptor circuits are formed by the twisted-pair wires (G-G' and 1-2). In this case, only single wire of the generator circuit is driven. From the circuits shown in the figure, the receptor differential voltage can be found as

$$V_{SR} = \left[\frac{Z_{SR}}{Z_{SR} + Z_{LR}}\right] j\omega dz \left[(L_{G1} - L_{G2})(I_{G1} + I_{G3} + \ldots) - (L_{G'1} - L_{G'2})(I_{G2} + I_{G4} + \ldots)\right]. \qquad \text{(IIID-3)}$$

One would notice that the drop of the voltage in (IIID-3) from (IIID-2) depends on the neutralizing mutual inductance (NMI) term ($L_{G1} - L_{G2}$).

Similarly, the receptor differential voltage for the STS/TWP model, as shown in Fig. IIID-1(c), is given by

$$V_{SR} = \left[\frac{Z_{SR}}{Z_{SR} + Z_{LR}}\right] j\omega dz (L_{G1} - L_{G2})(I_{G1} - I_{G2} + I_{G3} - \ldots). \qquad \text{(IIID-4)}$$

As the assumption made on the equality of the current on each section,[18] V_{SR} in (IIID-2(c)) will be formed by single current generator (SCG) I_{G1} if the number of twisted-pair sections is odd.

For the circuits shown in Figs. IIID-1(d) to 1(f), both generator wires are driven differently by using differential input sources. The use of differential signaling technique, also known as balanced input, has distinct advantages in providing immunity to noise pickup and crosstalk between channels. It is based on the fact that the signal of interest generates equal but opposite currents on a balanced pair of wires while cross couplings are induced equally in receptor wires but in the opposite direction. The generator-receptor circuits in these figures can also be classified as straight-through differential-generator, straight-through receptor (STD/STP); twisted-pair differential-generator, twisted-pair receptor (TWPD/TWP), and straight-through differential-generator, twisted-pair receptor (STD/TWP). Fig. IIID-1(d) shows the STD/STP model where the generator circuit is driven by a differential input signal causing the two coupling voltage sources with opposite direction on the receptor wires. The receptor differential voltage is given by

$$V_{S12} = \left[\frac{Z_{SR}}{Z_{SR} + Z_{LR}}\right] j\omega dz \{(L_{G1} - L_{G2}) - (L_{G'1} - L_{G'2})\} \cdot (I_{G1} + I_{G2} + I_{G3} + \ldots). \qquad \text{(IIID-5)}$$

One can observe that the NMI term (L_{G1}-L_{G2}) can cause V_{SR} to reduce as compared to V_{SR} given in (IIID-2) for the untwisted-wire cases.

The TWPD/TWP model shown in Fig. IIID-1(e) is the most common configuration for the UTP-CAT5 cable where both generator and receptor circuits are formed by the twisted-pair wires. In this case, both wires of the generator circuit are driven. The receptor differential voltage can be easily given by

$$V_{S12} = \left[\frac{Z_{SR}}{Z_{SR}+Z_{LR}}\right] j\omega dz\{(L_{G1}-L_{G'1})-(L_{G2}-L_{G'2})\}\cdot(I_{G1}+I_{G2}+I_{G3}+\ldots). \qquad \text{(IIID-6)}$$

One can simply see that the voltage across receptor wires derived in (IIID-6) is as same as that given in (IIID-5).

Finally, consider the STD/TWP model shown in Fig. IIID-1(f), which consists of untwisted generator pair and twisted receptor pair, where the receptor differential voltage is expressed as

$$V_{S12} = \left[\frac{Z_{SR}}{Z_{SR}+Z_{LR}}\right] j\omega dz\{(L_{G1}-L_{G2})-(L_{G'1}-L_{G'2})\}\cdot(I_{G1}-I_{G2}+I_{G3}-\ldots). \qquad \text{(IIID-7)}$$

Compare to the expression of V_{SR} in (IIID-4), I_{G1} is also only a contributor. Furthermore, the equivalence of (L_{G1}-L_{G2}) and ($L_{G'1}$-$L_{G'2}$) could cause V_{SR} even lesser.

From the above analytical models, one would notice that the voltages V_{SR} in (IIID-5) through (IIID-7) are equal those in (IIID-2) through (IIID-4) with an additional NMI terms. Also, it should be noted that all circuits discussed above use the balanced load configuration for the generator and receptor circuits. This type of configuration can give the results without any complicated modeling of the "floor" coupling effect.[18] As a result, the contribution to the crosstalk on the receptor is mainly from the inductive coupling between the generator and receptor wires.

Topological Network Approach

A typical computer network under study is shown in Fig. IIID-2(a), where its constituents include a server hub, computers, and UTP-CAT5 cables consisting of a bundle of

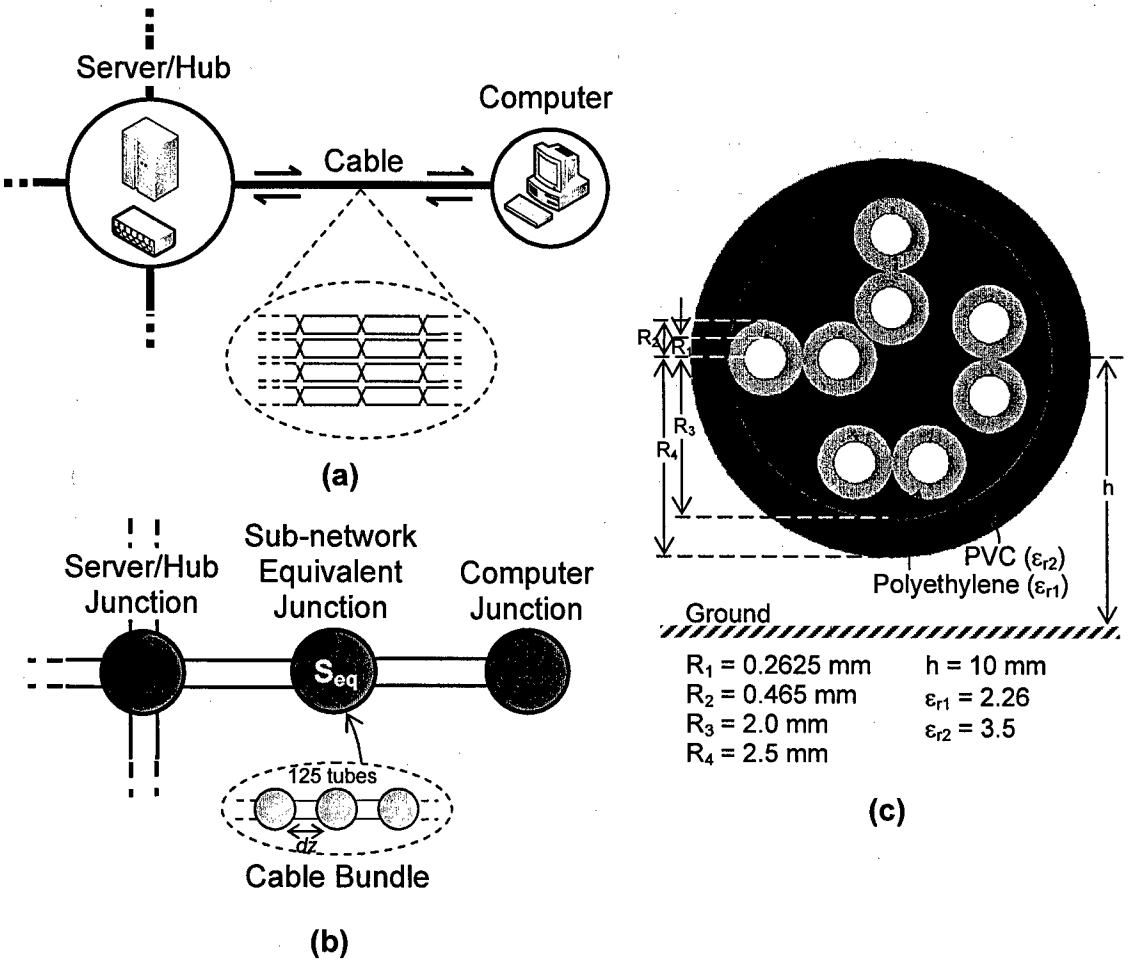

Fig. IIID-2 (a) Simple configuration of computer network and (b) associated topological network composed by junctions and tubes. (c) Cross-sectional view of the UTP-CAT5 cable consisting of four-pair conductors.

eight conductor wires. The associated topological network is shown in Fig. IIID-2(b), where it can be topologically decomposed into sub-volumes (junctions) interacting to each other through preferred paths (tubes). The junctions represent loads, branching of cables, or input impedance of electronic systems in the computer housings. The input and output waves are related to each other through a scattering matrix. The tubes between two junctions represent

the homogenous sections of cable harness based on the multiconductor transmission line theory. The per-unit capacitance, inductance, and characteristic impedance matrices generated from the companion LAPLACE code are used to characterize the tube. The traveling waves at each end are related to each other through a propagation matrix. Based on the multiconductor transmission line concept with scattering parameters at junctions and propagation parameters along tubes, the cable signals can be obtained through the BLT equations,[20] given by

$$\{[I]-[S][\Gamma]\}.[W(0)]=[S].[Ws], \qquad \text{(IIID-8)}$$

where [I], [S], and [Γ] are the identity, network scattering, and propagation supermatrices, respectively. The terms [W(0)] and [Ws] are the outgoing and source wave supervectors, respectively. The general solution of the BLT equations is in frequency domain. The advantage of using the EMT technique is that all volumes will be treated independently from others.

Cable Simulation Setup

The per-unit values of cable parameters were obtained from an electrostatic calculation using the LAPLACE code based on the Method of Moments application, by meshing different sections of the multiconductor cable for capacitance and inductance matrices.[21] The cross-sectional configuration and details of the cable are shown in Fig. IIID-2(c), where it consists of eight dielectric-coated cylindrical conductors held together in four pairs and resided in the cable jacket. Each of eight conductors was also designed with the per unit length resistance of 100 mΩ/m. Each circular contour for the conductor and dielectric surface was defined with 10 expansion functions (1 + 9 cosine terms) and a triangular contour for the ground plane was defined with 30 linear distribution functions.

Sub-network Compaction

In the simulations, the tube representing a 5-m long cable was decomposed into 125 tubes of homogenous sections with a length of 4 cm each. The junction characterizes the connection between two 4-cm tubes, which can be direct or twisted type corresponding to the circuit configurations shown in Fig. IIID-1. Since the entire length of cable comprises a large number of junctions and tubes with as many as eight conductor wires, direct calculation using the BLT equations is hardly cumbersome and time consuming. The matrix size required for such an exercise is large ($2 \times 8 \times 125 = 2000$), i.e. 2-directional junction, 8 conductor wires, and 125 tubes. If we were to assume that signals of interest are the waves traveling in and out the load junctions (concept of junction scattering), then it is possible to represent the whole cable network as a single equivalent junction, as shown in Fig. IIID-2(b). As a result, the original matrix reduces to $2 \times 8 \times 2 = 32$, decreasing computation time considerably. In addition, to realize a topological network with different terminal equipment, one needs only to change the boundary junctions without working out the entire topological network. With this setup, simulations were carried out to predict the near end crosstalk under various influencing parameters such as the value of the source and load impedances, the conductor pair location, and the cable driving source. The NEXT values were determined through (IIID-1) using crosstalk models related to (IIID-2) through (IIID-7) by applying a test signal to one cable pair and measuring the amplitude of the crosstalk signals received by the other cable pairs.

Crosstalk Reduction

The computed results in Fig. IIID-3 show the NEXT levels (1 kHz – 100 MHz) induced on the receptor pair 3-4, when the terminating impedances are 1 Ω and 1 kΩ. Shown in Fig. IIID-3(a) are the results using the STS/STP, TWP/TWP, and STS/TWP models when the generator wire 1 is driven by a 0.5 V source. Figure IIID-3(a) shows linear curves at low frequencies and standing waves at high frequencies. One can see that the crosstalk

induced on the receptor wires is higher when the terminating impedance is 1 Ω, e.g. at low frequencies, the value of curve 1 is approximately 16-dB higher than that of 15 kΩ (curve 4) for the STP/STP model. The reason is that, regardless of the capacitive coupling due to the balanced-load configuration, the inductive coupling is dependent on the generator current. The low impedances on the generator wire could result in a high value of current generated. Another observation is that the STS/TWP model provides the best in crosstalk reduction while the STS/STP model gives the worst performance. In other words, twisting either the generator or receptor pairs improves the effectiveness of crosstalk reduction, i.e. at 1 kHz and 1 Ω, the NEXT value of the STS/STP model is -60 dB while the STS/TWP's is approximately -100 dB. The different performances of crosstalk suppression can be directly explained by expressions given in equations (IIID-2) through (IIID-4). The introduced NMI term in (IIID-3) and SCG effect in (IIID-4) cause the reduction of the induced voltage. Simulations also showed that the multiconductor transmission line based simulation is less consistent when the length of the cable is considered electrically long or when curves enter the frequency of standing-wave region at above 1 MHz.

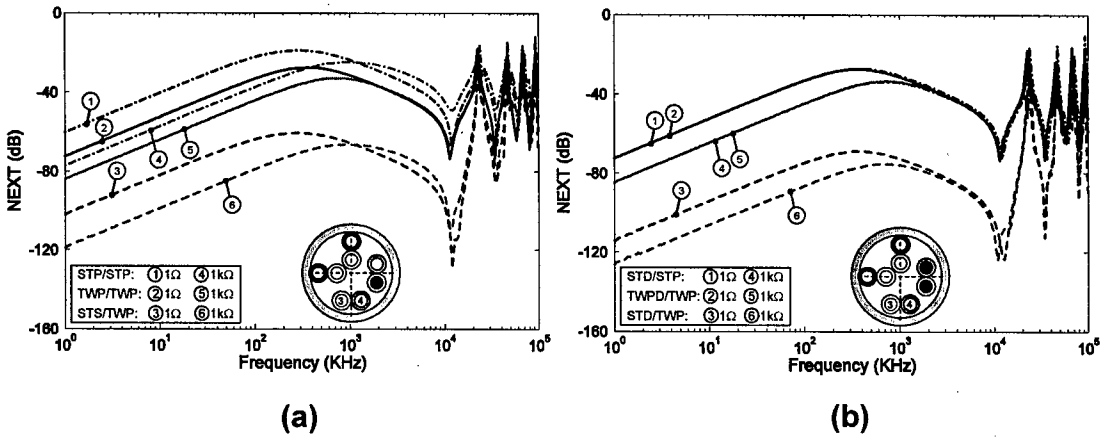

Fig. IIID-3 NEXT levels across conductors 3 and 4 as a function of the source and load impedances (1 Ω and 1 kΩ) in frequency domain for coupling circuits driven by (a) + 0.5 V source on conductor 1 and (b) ± 0.5 V on conductors 1 and 2.

The next simulation examines the effects of using the balanced input technique. The results are compared with those obtained by driving a single wire generator. The computed NEXT results on the receptor pair 3-4 using the STD/STP, TWPD/TWP, and STD/TWP models are shown in Fig. IIID-3(b) when the generator wires 1 and 2 are driven respectively by +0.5 V and -0.5 V sources. Compared with the results presented in Fig. IIID-3(a), one can see the enhancement in crosstalk reduction. The enhanced performance of the NEXT suppression associated with curves 1, 3, 4, and 6 is due to the neutralizing mutual inductance created by the second driven generator wire. The improvement of crosstalk reduction is hardly noticeable for curves 3 and 4. Analysis of the results from the simulations are consistent with the analytical expression of all models derived from equations (IIID-2) through (IIID-7). Clearly, twisting either the conductor pairs introduces the SCG-type enhancement while balancing the input signal introduces the NMI term. The same can be said for the receptor pairs 5-6 and 7-8 as the associated computed results can be seen in Figs. IIID-4 and IIID-5, respectively, for both types of driving signals.

Since the crosstalk circuit model used in this work were analytically analyzed without

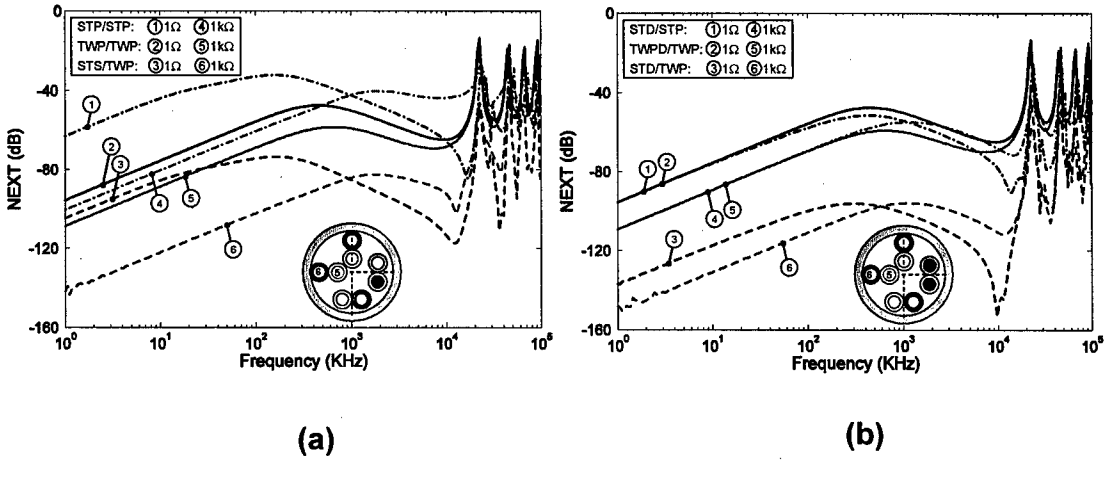

Fig. IIID-4 NEXT levels across conductors 5 and 6 as a function of the source and load impedances (1 Ω and 1 kΩ) in frequency domain for coupling circuits driven by (a) + 0.5 V source on conductor 1 and (b) ± 0.5 V on conductors 1 and 2.

considering the dielectric coating as well as the transmission line loss. As a result some discrepancy is expected between the analytical results and the EMT calculations, which account for the non-homogenous media and the current attenuation associated with the computer code-modeled UTP-CAT5 cable.

Related Publications

Related works to this interaction study are reported in the paper [2006J1] and technical report [2006C1].

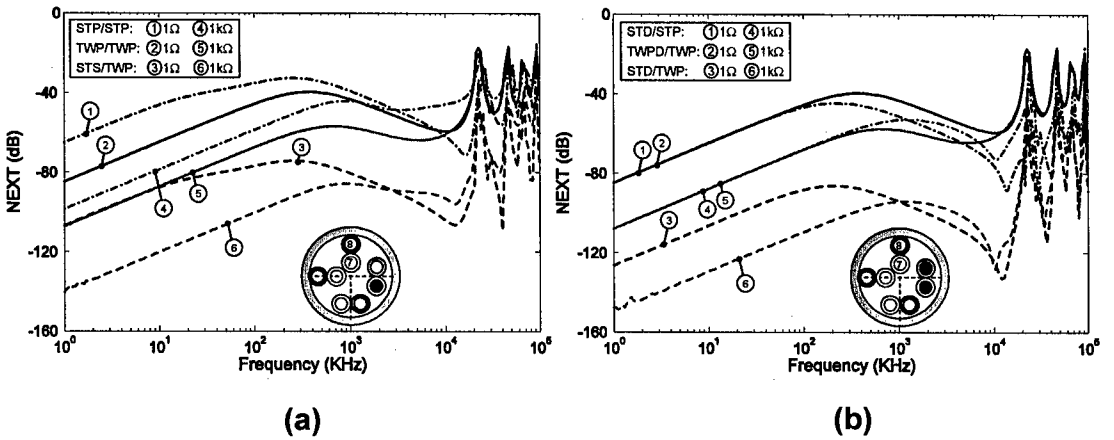

Fig. IIID-5 NEXT levels across conductors 7 and 8 as a function of the source and load impedances (1 Ω and 1 kΩ) in frequency domain for coupling circuits driven by (a) + 0.5 V source on conductor 1 and (b) ± 0.5 V on conductors 1 and 2.

(E) Interaction Studies: Heating of Semiconductor Devices and Structures

Photoconductive semiconductor switch (PCSS) is an important component of the Ultra Wideband (UWB) High Power Microwave (HPM) generation circuitry. It has been utilized for the generation of microwave energy at DE at AFRL, NM. Generation of

microwave energy source is important since many of the defense programs depend on microwave energy for communication and/or sensing. Research at UMC-Columbia has contributed greatly to the successful characterization of compact PCSS fabricated from 6H-SiC, in close collaboration with Lawrence Livermore National Laboratory (LLNL). This is in line with our previous effort, which included analysis of GaAs PCSS for use at DE/AFRL, NM.

Compact HPM generators using technology described earlier can be easily transported and directed against critical electrical systems. In order to guard against such attacks, a thorough understanding of the RF/System interaction, which can be utilized for both offensive and defensive purposes, is required. High power electromagnetic pulse on systems can result in heating the device structure and the contact regions. A change in the permittivity parameter may occur. The main objective of the research therefore is to test, simulate, and develop process and device technologies that directly affect the performance of photoconductive switches used in high power microwave generation and to protect electrical systems from harmful effects of electromagnetic pulses and lightning. This is best achieved by non-destructive analysis such as simulation studies using codes. The ECE department at the University of Missouri-Columbia is developing a comprehensive plan for the testing of effects of electromagnetic illumination of solid-state devices and the accompanying circuitry, specifically those designed for RF application.

Device Geometry and Materials

The GaAs PCSS simulated is operated in the non-linear mode with length and depth of 2700 and 630 μm respectively. It is a truncated version of the device used in the UWB HPM circuitry shown in Fig. IIIE-1. The Pd contacts are diagonally opposed, as shown in Fig. IIIE-2(a). The distance between the contacts is 0.25 cm, which is similar to the original device. The contact region has been truncated to 100 μm (will require lesser computer time)

and since the active region has not changed, the response is expected to be similar to the original device. The device material is deep-donor-shallow-acceptor (DDSA) compensated type with 3×10^{15} atoms/cc carbon compensated by EL2 donors at 0.370 eV. The EL2 donors are also a trap site. The electron and hole capture cross sections were 4×10^{16} atoms/sq.cm and 2×10^{18} atoms/sq.cm respectively. The bulk resistivity is of the order of 10^7-10^8 Ω-cm. Details on the structure has been published elsewhere.[22]

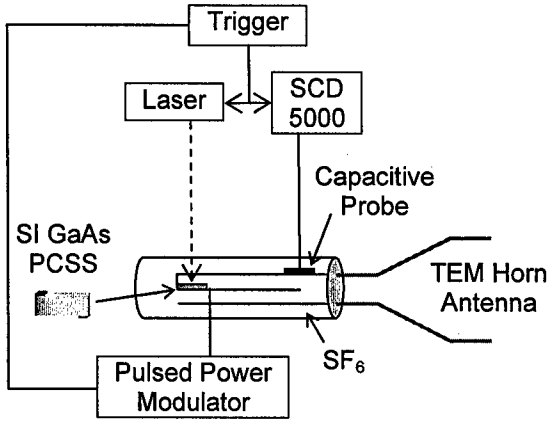

Fig. IIIE-1 UWB radiation source setup and opposed contact PCSS.

The 6H-SiC PCSS used for the simulation is shown in Fig. IIIE-2(b). The length and the width of the device are 1.2 cm x 1.2 cm and is approximately 350-400 μm deep. The radius of contact curvature is 0.2 cm. The contact leaves the 6H SiC slab around 0.4 cm from the center of the switch. The Nickel Silicide contacts have resistivity of about 1×10^{-5} Ω-cm.[23] The actual contacts are made up of NiSi2/Ti/Pt/Au layers with thicknesses 200/200/100/100 nm respectively, followed by a 1000-μm Copper (Cu) layer. Since only the material in intimate contact with SiC is expected to affect the injection behavior Nickel Silicide is only used for the simulations. 2D device with ~8000 mesh points was generated in the simulation

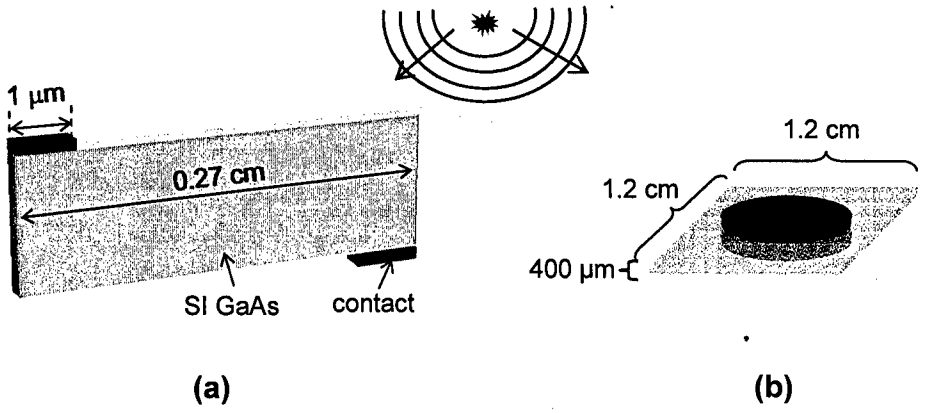

Fig. IIIE-2 Semi-Insulating PCSS. (a) GaAs with Pd contacts and (b) 6-H SiC with Ni contact.

mesh.[24]

SILVACO Simulation Setup and Results

Models required for simulations include the mobility and recombination parameters, their dependency on the electric field in different regions of the device. Poisson's and carrier continuity equations were solved in the semiconductor regions using equations as shown,

$$div(\varepsilon \nabla \psi) = -\rho \qquad \text{(IIIE-1)}$$

$$\frac{\partial n}{\partial t} = \frac{1}{q} divJ_n + G_n - R_n \qquad \text{(IIIE-2)}$$

$$\frac{\partial p}{\partial t} = \frac{1}{q} divJ_p + G_p - R_p, \qquad \text{(IIIE-3)}$$

where q is the magnitude of the charge on an electron, n and p are electron and hole concentrations respectively, J_n and J_p are electron and hole current densities, G_n and G_p are generation rate of electron and holes, R_n and R_p are recombination rates for electrons and holes.

Lattice temperature effects were incorporated using the Wachutka's thermodynamically rigorous model of lattice heating. This accounts for Joule heating and cooling due to carrier generation and recombination, and the Peltier and Thomson effects. The heat flow equation has the form

$$C\frac{\partial T_L}{\partial t} = \nabla(\kappa \nabla T_L) + H, \qquad \text{(IIIE-4)}$$

where C is the heat capacitance per unit volume, κ is the thermal conductivity, H is the heat generation and T_L is the local lattice temperature. Along with the charge carrier transport equations, following assumptions are made. 1) Even if the device temperature is driven far away from thermodynamic equilibrium, electron and hole subsystem is in local equilibrium. The electron and hole states can be found out by the local temperature and quasi Fermi level and states of the host lattice atoms can be determined by host temperature T_L. The three systems exchange energy by various scattering mechanisms. The lattice scattering is responsible for energy transfer between free carriers and substrate. Carrier-carrier scattering transfers energy electrons and holes. Also various recombination and generation processes, SRH, Auger are evoked in the analysis. Energy is also exchanged between the carriers and ambient via radiative recombination and optical generation and is also considered in the modeling. 2) All hot carrier effects are neglected. 3) Thermal conductivity does not change with increase in temperature.

In order to define a critical heat source location for detailed studies, a number of initial simulations were carried out by changing the location of the heated region on the devices. Locations heated to 330 K included the device contacts (anode and cathode) and different regions on the PCSS body. This was done because the device responses are expected to depend on the location of the heat source and the nature of carrier flow in that region. In every simulation the device IV-characteristics was monitored. For contact heating, it was

found that an anode as a heat source presented the worst case for device failures. This configuration was therefore chosen for detailed studies.

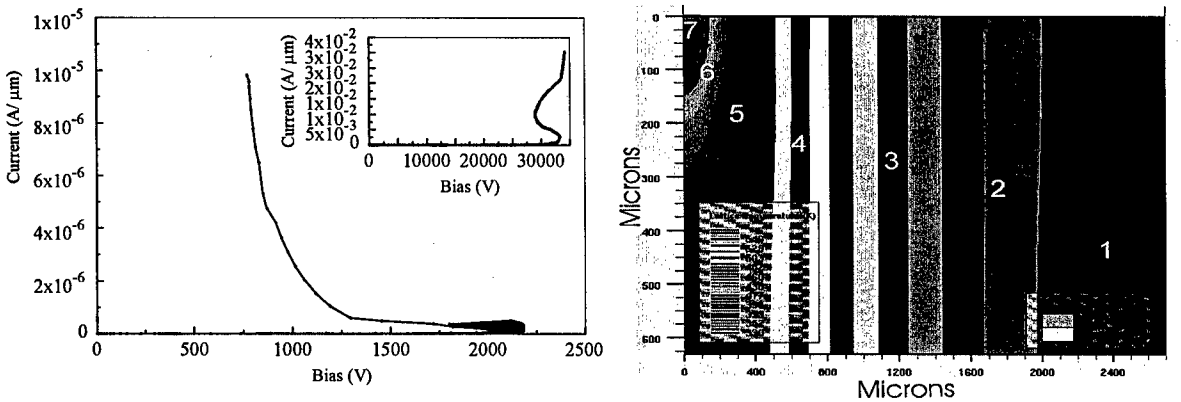

Fig. IIIE-3. (a) Characteristics of the opposed contact PCSS before and after heating. (b) Temperature distribution due to heating. Regions 1: 560 K, 2: 550 K, 3: 525 K, 4: 503 K, 5: 460 K, 6: 438 K, and 7:395 K.

An IV plot for the opposed contact GaAs, with anode heated, is shown in Fig. IIIE-3(a). The figure has two important characteristics. First, device breaks down at a much lower bias when heated than without a heat source on the device. Secondly, the device exhibits negative resistivity like conduction at a voltage much lower than the operating voltage. This current controlled negative characteristics leads to filamentary conduction and is inherently unstable.[25] The temperature profile in the device, prior to breakdown is shown in Fig. IIIE-3(b). As expected, thermal generated carriers near the electrodes contribute to excess current generated negative resistivity behavior. As a result, filamentation conduction shifts to a much lower voltage (shown in Fig. IIIE-3(b)). The filamentation process can be expected follow the usual path of nucleation growth, followed by the growth of a second filament within the first filament. The filamentation begins in a region of high current density and more than one filament may occur and the device is irreversibly damaged. The process of charge controlled negative resistivity behavior and filamentation has been discussed in detail

by Gandhi.[25]

Fig. IIIE-4(a) shows the response of the SiC PCSS with the anode heated at 330 K. Switch breakdown occur at a voltage that is much smaller than the GaAs PCSS, even though its non-heating breakdown occur at voltages that is much higher than that of the GaAs PCSS (Fig. IIIE-4(b)). This behavior could be attributed to the better thermal conductivity of SiC. In the absence of a heat sink, one does not expect heat dissipation in the device, which leads to failure.

Related Publications

Related works to this interaction study are reported in the paper [2006J2] and technical report [2005C4].

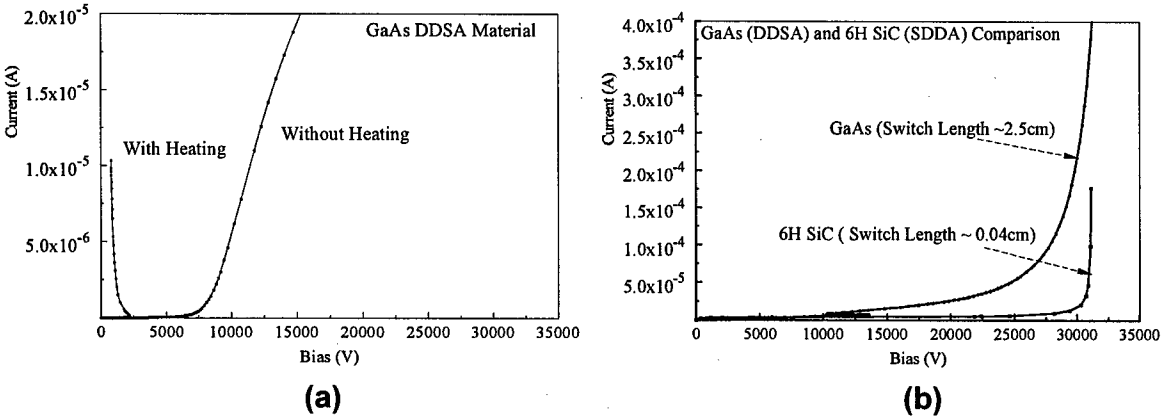

Fig. IIIE-4 (a) Effects of anode heating (330 K) on SiC characteristics. (b) Breakdown characteristics of GaAs and SiC PCSS.

(F) Interaction Studies: Fields Analysis of Enhanced Charge Collection in Nanoscale Grated Photo Detectors

The simulation method is based on the Finite Integration Technique (FIT) which provides a discrete reformulation of Maxwell's equations in their integral form suitable for

computers for electromagnetic field problems with complex geometries. The associated integral form of a grid cell surface can be written by the differential equation

$$e_x(i,j,k)+e_y(i,+1,j,k)-e_x(i,j+1,k)-e_y(i,j,k)=-\frac{d}{dt}b_z(i,j,k), \qquad \text{(IIIF-1)}$$

where the scalar value $e_x(i,j,k)=\int_{(x_i,y_j,z_k)}^{(x_{i+1},y_j,z_k)}\vec{E}\cdot d\vec{s}$ represents the exact value of the integral over the distance of the electric field and the scalar value $b_z(i,j,k)=\int_{A_z(i,j,k)}\vec{B}\cdot d\vec{A}$ represents the integral over the area of the magnetic flux density. Simulation equations using this technique are incorporated in a commercial code that has been used in this analysis.[26] The FIT based simulation in this study is analyzed as to confirm with the results obtained from measurements of nanoscale semiconductor devices (photodetectors) with different grating structures.

Metal-semiconductor-metal Photodetector

A photodetector (PD) is an important component of an optical transmission and measurement system. For fast and reliable operations such systems require detectors with high efficiency, good responsivity and wide bandwidth. A class of device known as the metal-semiconductor-metal (MSM) photodetector meets these requirements and has been widely used in many optical and measurement systems.[27] MSM PD is a planar device with Schottky barriers on either side of an exposed semiconductor absorption region. It requires low fabrication processing steps and has high speed because of low capacitance. The electrodes in these devices are often interdigitated to increase the active region area while optimizing the electric fields in the carrier collection region.

CST Microwave Studio Simulation Setup and Results

The simulation scheme is shown in Fig. IIIF-1(a). In this setup, a section of the detector with three grating structures (wall, square, cone, and hatched-top cone), each 1.8-μm in height, are to be simulated and compared for analysis. The transmission of a *z*-polarized incident wave through the structures will generate changes in the wave amplitude as it crosses the region, into the active area. These plots will be compared for analysis, first to determine the best structure shape that will allow for maximum energy transmission and later, once the shape is determined, it height will be optimized. Fig IIIF-1(b) shows a

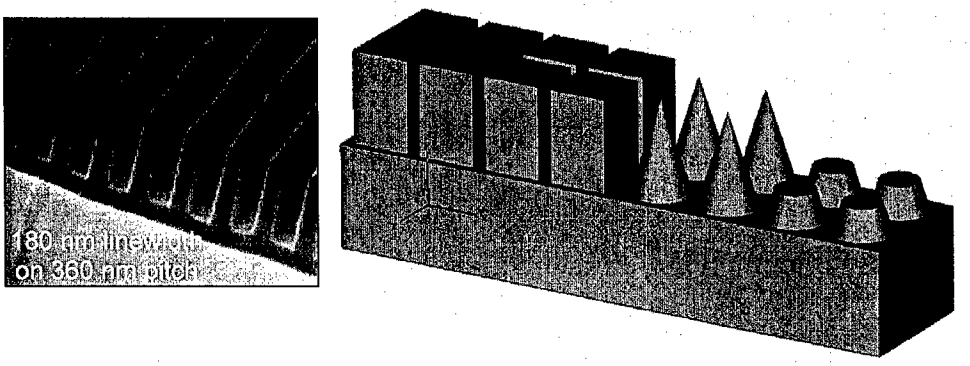

(a)

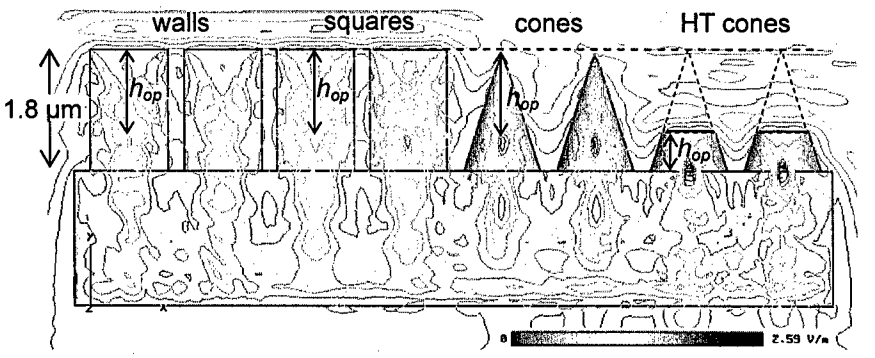

(b)

Fig. IIIF-1 (a) Bulk Si detector with different 1.8-μm tall grating structures, i.e. square, cone, and hatched-top cone. The inset shows the wall grating-type detector from experiments. (b) Maximum isoline plot of the incident wave transmitted through substrate, square, cone, and hatched-top cone structures. The curves display the optimum height, h_{op}, of each structure.

maximum isoline plot of the four shapes in 2D plane. It shows that the hatched-top cone has the highest E-field close to the active region while the wall-type grating has the lowest maximum peak. This suggests that grating structures as a square, cone, and hatched-top cone have similar effects as that of a wall-like grating (inset Fig. IIIF-1(a)) structure, and would contribute towards enhancing charge collection as was demonstrated earlier.[28]

For simulations a 10×10×2 μm Si region, representing a section of the detector's active region, was used in the simulations as shown in Fig. IIIF-2(a). A 1 V/m plane wave port as the source in the negative *y*-direction with continuous sinusoidal wave was also used as the

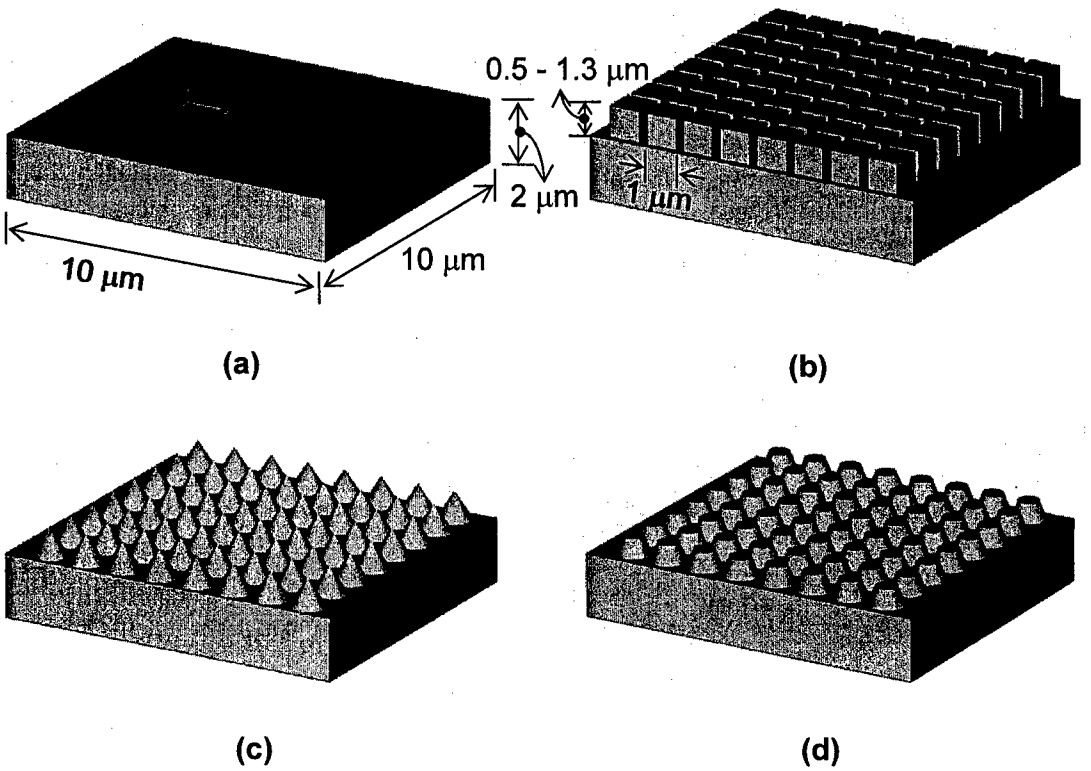

Fig. IIIF-2 Configurations of MSM photodetectors used in simulations. Structures are a 10×10×2 μm Si-substrate (a) without gratings, (b) square gratings, (c) cone gratings, and (d) hatched-top cone gratings.

excitation signal. For Si, it is also important that the incident wave have energy equal to or greater than the material bandgap and hence is capable of creating electron-hole pairs at the interface. Wave length corresponding to the bandgap energy was therefore chosen for our simulations. In order to optimize the gratings shape for maximum transmission, different geometry (i.e. square, cone and hatched-top cone), were chosen for comparison as shown in Figs. IIIF-2(b), IIIF-2(c), and IIIF-2(d). E-fields were monitored by placing probes at the interface between the grating and the Si substrate. Due to changes in structural shape and the effects refraction and transmission there is a change in the transmission coefficient (transmitted energy) as it passes from one region to another. Simulation results to optimize the transmitted energy are discussed in subsections A, B, and C. Results from SiO_2 cladding on the gratings is also included in the discussions.

Optimization by varying height of the gratings

Structures shown in Fig. IIIF-2 were simulated by varying the heights of the gratings from 0.5-1.3 μm., while the area covered on the active region was kept the same for all the structures. The plots of normalized E-field amplitude associated with square, cone, and hatched-top cone structures with different heights are shown in the Fig. IIIF-3(a). One can see that each structure has unique optimum height, h_{op}, with the square, cone, and hatched-top cone having optimum heights of 1.0 μm, 0.9 μm, and 0.6 μm, respectively. The hatched-top cone structure of Fig. IIIF-2(d) shows maximum normalized amplitude of 2.45 at a height of 0.6 μm as shown in Fig. IIIF-3(b). Since transmitted amplitude contributes to transmission coefficient (which effects transmitted power), this structure therefore allows for maximum energy transfer into the substrate. The fabrication cost is also expected to be the least for this structure due to its low height h_{op}.

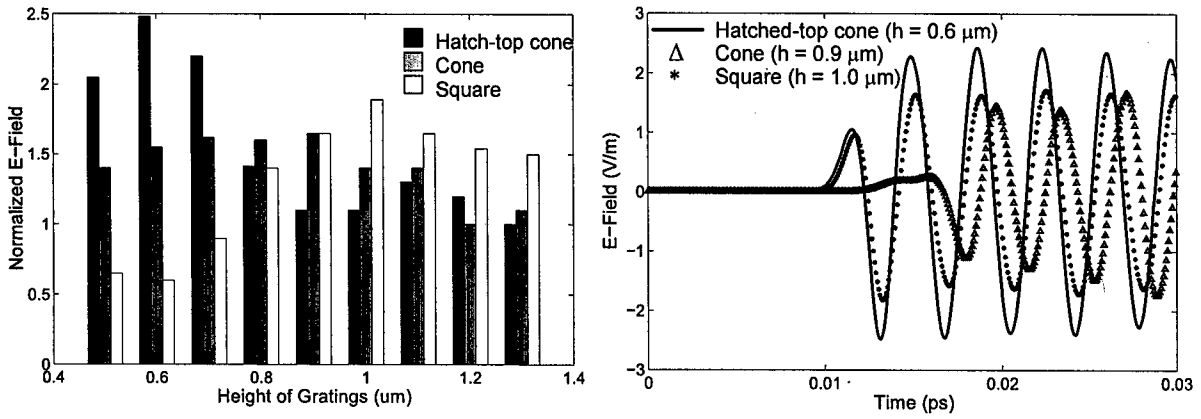

Fig. IIIF-3 Normalized (with 1 V/m) E-field peak associated with square (white), cone (gray), and hatched-top cone (black) structures as a function of height. (b) E-field vs. time waveforms of three structures associated with their optimum heights. (solid line: hatched-top cone with height = 0.6 μm, triangles: cone with height = 0.9 μm, and asterisks: square with height = 1 μm).

In cases of wall, square and cone, the focus point is not so close to the active region. Also as the height is increased, the focus point shifted slightly to the top and thus there is a decrease in the E-field. Thus the high transmitted amplitude for the hatched-top cone as compared to the other two structures could be due to a combination of the effects of slant-side and flat-top surfaces that result in focusing the transmitted waves on one particular spot close to the top surface. As a result, the hatched-top cone structure has high E-fields. Further analysis in this paper is therefore dedicated to the hatched-top cone structure.

Optimization by varying number of gratings on the active region

Number of grating structures on the active region was varied to optimize the charge collection. This effectively changed the area covered by the gratings while keeping the area of the active region constant i.e. the percentage of area covered by the Si gratings on the active region changes. The dimension of each grating structure is kept constant at a μm^2 where a is the area covered by each grating structure on the active region. Hence, the entire area covered by the gratings is na μm^2 (n = number of gratings).

The relationship between the number of gratings and the normalized E-field peak for the hatched-top cone structure is shown in the Fig. IIIF-4. The maximum E-field corresponds to 100 hatched-top gratings. The E-field magnitude starts at low value and then slowly increases till a critical number of gratings is reached and starts reducing again. This is because, for smaller number of gratings, the distance between the structures is larger than the wavelength and the there is no contribution from adjacent regions. As the number of gratings increases, the separation distance between the gratings decreases which cause multiple constructive interference similar to the one described earlier. This causes the E-field magnitude to increase. As the number of gratings increases further, the E field starts to decrease. The reason is that a large number of clusters make the region behave as a bulk region.[29]

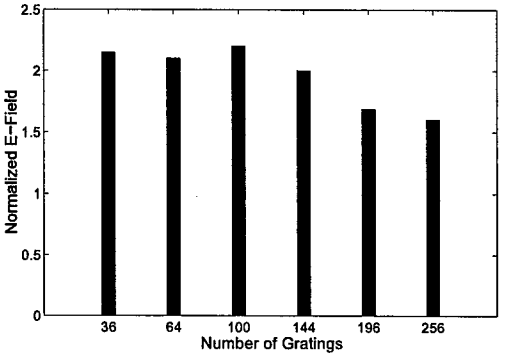

Fig. IIIF-4 Relationship between the number of gratings and the normalized E-field peak for the structure with hatched-top cone gratings.

Optimization of the charge collection by using a cladding of SiO_2

Finally, changes in the transmitted E-field magnitude were studied with SiO_2 layers on the grating surface. Oxides grow naturally on exposed Si surfaces primarily due to the interaction of Si dangling bonds with oxygen in air. Most practical devices are expected to have such a layer. A hatched-top cone grating, which generated the optimum E-field amplitude in the active region, was used in the simulation (Fig. IIIF-5(a)). The oxide thickness on the grating surface was about 0.05 μm. Again, the E-field probe was placed at the interface between Si in the active region and the gratings. A comparison of Fig. IIIF-3(b) and Fig. IIIF-5(b) shows that there is no significant difference in the E-field amplitude with the oxide layer on top of the optimum height (0.6 μm, hatched-top) structure. In order to

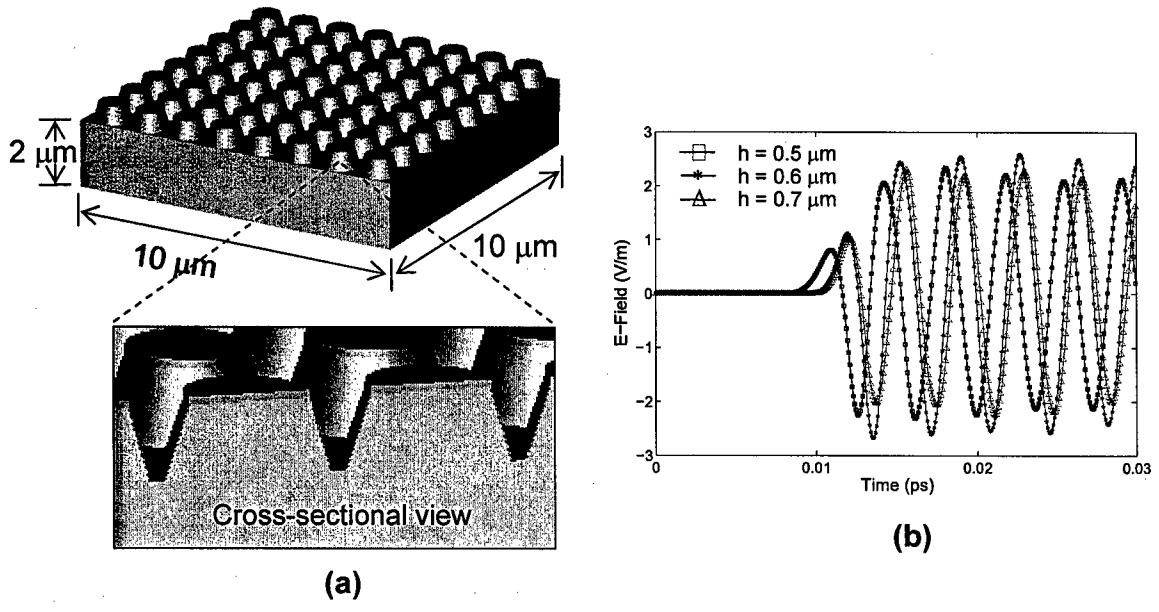

Fig. IIIF-5 Structure consists of a 10×10×2 μm Si substrate. The Si hatched-top cone gratings on top of the bulk SiO_2 are coated with SiO2 layer of 0.1 μm thicknesses. (b)Waveforms of E-fields of the structure consisting of hatched-top cone Si and SiO_2 coating with different heights (squares: 0.5 μm, Asterisks: 0.6 μm, and triangles: 0.7 μm).

determine a new optimum height, the structure height was then altered to 0.5 and 0.7 μm respectively. No significant change in transmitted E-field amplitude was seen. However, improvements in transmission amplitude occur when the grating thickness is increased to a quarter wavelengths. This is shown in Fig. IIIF-6. The quarter wavelength thickness is expected to minimize reflection at the interface through destructive interference.

Related Publications

Related works to this interaction study are reported in the papers [2006J4] and [2005J1].

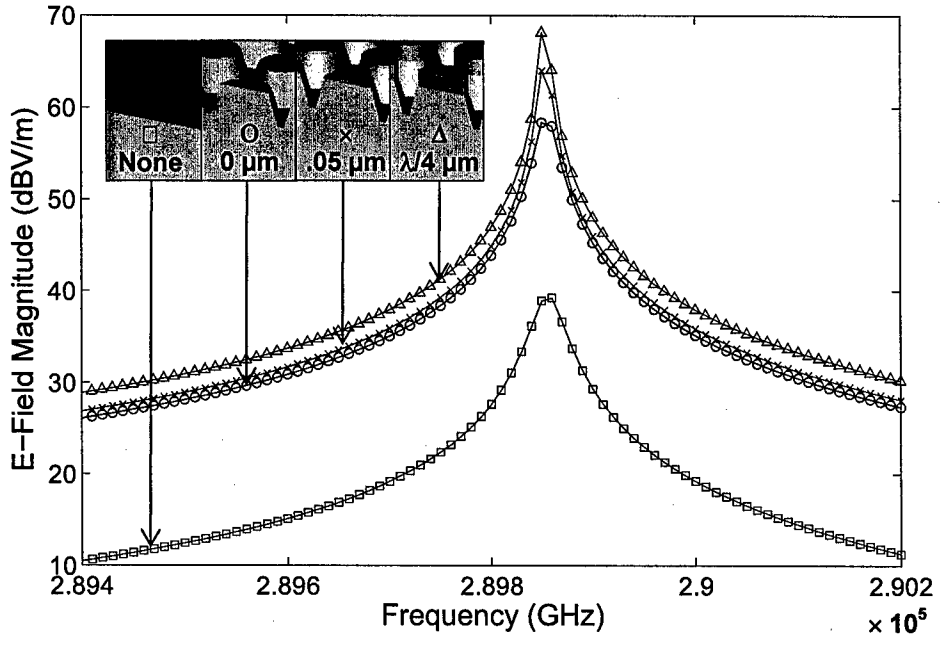

Fig. IIIF-6 E-field magnitude frequency components (dBV/m) associated with the substrate without gratings (Squares) and the substrate with three cladding thickness cases (Circles: 0 μm, Crosses: 0.05 μm, and triangles: 0.258 μm).

(G) Interaction Studies: TEM Cell Modeling

TEM cells are used in EMC laboratories for radiated immunity and emission testing of electronic devices, including biomedical-related samples such as human tissues and membranes. The EM wave propagation inside the cell has a free space impedance of 377 Ω. It, therefore, provides a close approximation of a far-field plane wave propagating in free space. The useful frequency range of a symmetrical 50-Ω TEM cell is limited by the cut-off frequencies of the higher-order modes and appearance of the resonances due to reflections at the taper-sections. Such resonances can destroy the field homogeneity.

In this report, we preliminarily study the TEM cell using FIT based simulations. The empty cell was modeled to investigate the uniform field as desired. Field perturbations and effects on the samples will be studied in the next phase.

TEM cell model and simulations

The model was implemented using the CST Microwave studio software. The cell consists of a section of rectangular coaxial transmission line tapered at each end to adapt to external N-type coaxial connectors. The detailed dimensions of the TEM cell used in the simulations are shown in Fig. IIIG-1. The effective frequency range is from DC to 200 MHz. The source was feeded from the front end by using a discrete port. It consists of a current source with an internal resistor. This kind of port is used as feeding point source or as the

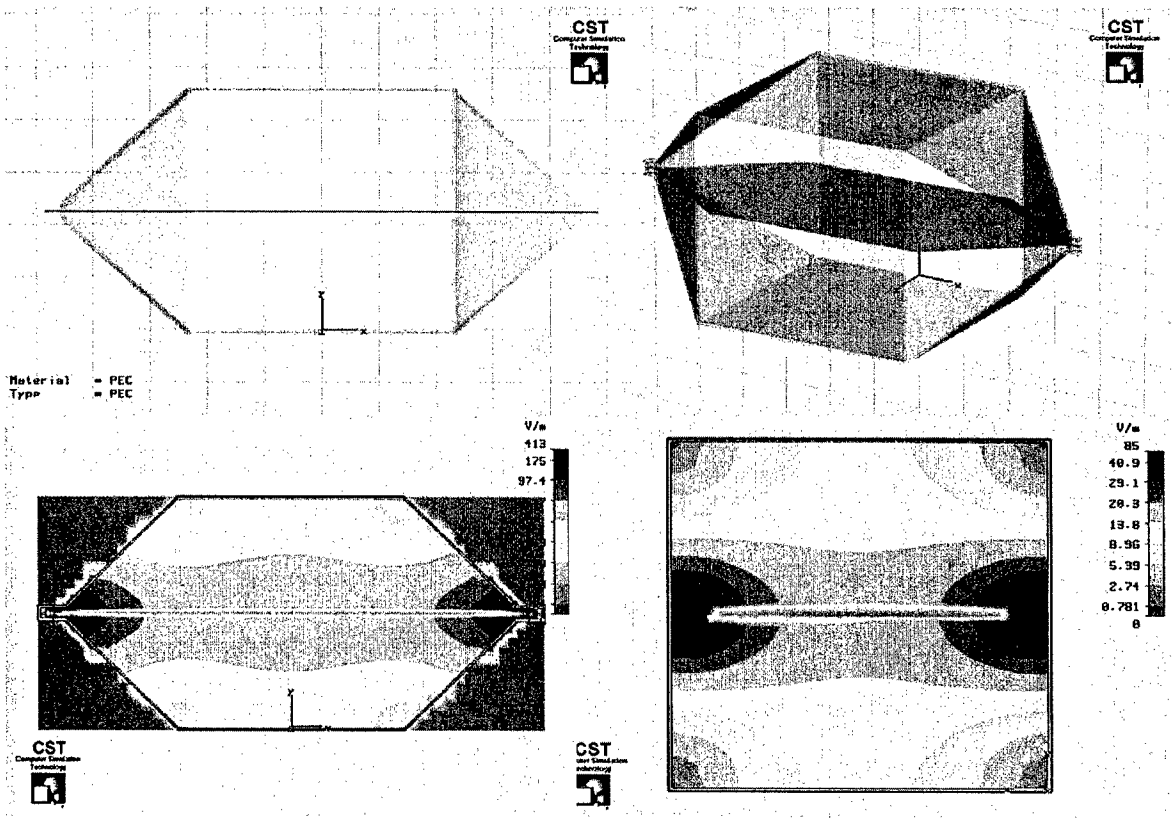

Cell dimension:	180×90×90 cm^3
Frequency range:	DC to 200 MHz
Septum:	74 cm (length)
	0.157 cm (thickness)

Fig. IIIG-1 Configuration and Electric Field distributions on side and front views of the TEM cell.

termination of the transmission lines at very low frequencies.

Simulation shows the uniform E-field distribution in the region of the center of the cell and less uniformity as the region gradually moves towards to the wall. This frequency of 50 MHz was chosen because only TEM mode dominates. This result suggests the region where a device should be inserted for radiated and conducted immunity testing.

(H) Experiments: Anechoic Chamber Electromagnetic Interaction Tests

Many methods for simulating electromagnetic interaction are in existence. The interaction under scrutiny in this report is the transmitted RF signal when an incident RF signal interacts with an aperture. The report will step through an example test in order to highlight the capabilities and limitations of the current test setup.

When considering the incident signal, it is necessary to consider the hardware available for testing. A summary of the hardware is below.

Equipment	Frequency Range	Power/Field
Control Computer	NA	NA
Signal Generator	9 kHz to 1.1 GHz	-140.0 dBm to 13 dBm
RF Amplifier	80 MHz to 1 GHz	0 dBm (max input) Gain +52 dBm
Log-periodic Antenna	80 MHz to 5 GHz	Gain 36 dBm
Semi-Anechoic Test Cell	27 MHz to 4.2 GHz	500 W
E-field Probe	100kHz to 3 GHz	.4 to 660 V/m

From this table, the acceptable test frequency range is 80 MHz to 1 GHz and the maximum E-field (RMS) should be roughly 10 V/m. The next step is choosing an incident signal.

Before choosing an incident signal, the limitations of the equipment should be considered. Practically speaking, the signal generator can only generate sinusoids with amplitude modulation, frequency modulation and phase modulation. However, if the signal

can be represented in the frequency domain by the Fourier transform, then a subset of the resulting frequency-amplitude pairs can be tested. Thus, the general procedure is to pick the incident signal in the time-domain, convert it to the frequency domain by using the Fourier transform, scale the amplitudes by $2^{-1/2}$ to get RMS amplitudes and select frequencies between 80 MHz and 1 GHz to be tested. The resulting frequency-amplitude pairs should be saved to a text file with the frequency in Hertz and the RMS amplitude in V/m separated by a tab, one per line. For this example, the frequency-amplitude pairs consist of a constant 10 V/m (RMS) at 80, 90, 100, 200, 300, 400, 500, 600, 700, 800, 900 and 1,000 MHz.

The next step is setting up the equipment for the test. The controlling computer, signal generator and amplifier should be turned on. The amplifier should be set to 100% gain. The antenna should be oriented so its polarization matches the polarization of the incident field. This step increases the probability that the desired field strength in the axis of polarization will be obtained. In this example, both antenna positions are tested for all three axes. The probe should be placed at the position of the incident aperture, aligned with the test cell and turned on. Currently, the manufacturer of the E-field probe includes a method for aligning the probe to the test cell. However, the method is tedious and error-prone so an alternative method of coordinate transformations is under investigation. The origin of the coordinate system of the test cell is the center of the antenna. From the perspective of standing behind the antenna looking into the cell, straight up is the positive x axis, straight right is the positive y axis and straight into the cell is the positive z axis. At this point, the test cell should be sealed and the testing procedure started.

The first step in testing is starting Measurement and Automation explorer and scanning the GPIB bus for instruments. The address of the signal generator should be noted for use later. After scanning for instruments, the test program should be started. All of the inputs to the program should be set before pressing the Start button.

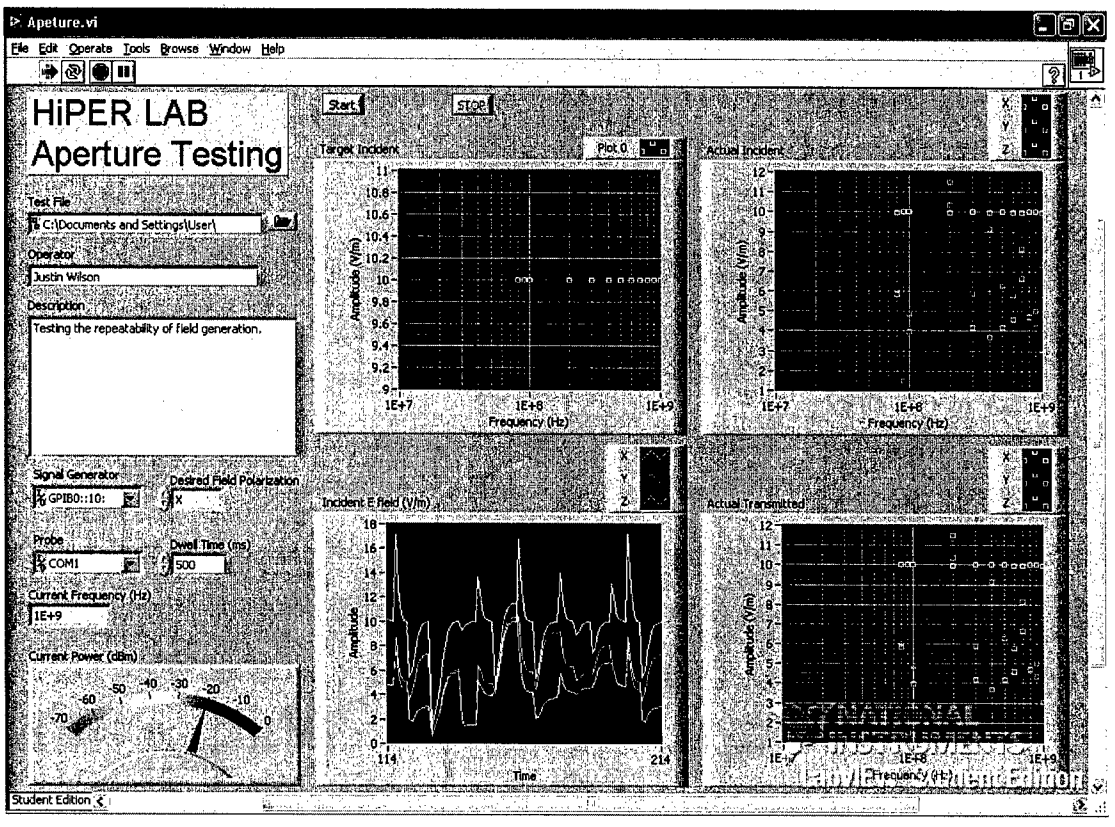

Fig. IIIH-1 LabVIEW control panel for aperture testing.

The inputs to the program are the name of file with the frequency-amplitude pairs, the name of the operator, the description of the test, the VISA address of the signal generator, the VISA address of the E-field probe, the desired field polarization and the dwell time. When the user presses start, the first action of the program is to read the file with the frequency-amplitude pairs into memory and plot the result (upper-left graph). The second step is the initialization of the chosen signal generator. The third step is the initialization of the probe. Initializing the probe takes some time due to a zeroing procedure. The fourth step is finding the necessary power levels to achieve the desired field strength in the desired field polarization dimension. During this step, the field strength of all axes is charted (lower-left chart). When this step is done, the actual incident field for each frequency is graphed

(upper-right graph). The fifth step is adding the aperture to the test cell. The sixth step is adjusting the generator to the necessary power and frequency for the time set in dwell time then measuring the E-field. At the conclusion of this step, the transmitted E-field vs. frequency is graphed (lower-right graph). The seventh step is the generation of a report file that includes the time and date, the name of the operator, the description and the frequency amplitude pairs (both desired and measured).

Before describing the results of the example test, some comments about how the program and test equipment are in order. The E-field probe is set to sample at 60 Hz and provide the RMS amplitude of the E-field in all axes. The software uses a 25-point average when considering one measurement. This option might be made available to users in the future. The only forms of control are the frequency and the power at the signal generator. These cause an E-field with x, y and z components to be generated in the test chamber. The frequency is fixed for the test so the only variable is the power setting. It is only possible to level the field in one dimension. This dimension is specified by the desired field polarization input.

To prove that the system can generate the required fields, the system can be run without an aperture. The expected result is that the incident field strengths will equal the transmitted field strengths. This experiment was conducted in each axis with both antenna positions using the sample file previously described. The probe was placed at (0, 0, 2.5m). It is expected that certain configurations will not be able to generate the required field. Remember that the probe axes and the test cell axes are not correspondent in this example. The results of this test are included in a table below. Of the two tests that generated the desired field without difficulty, the error between the desired field and the incident field and the desired field and the transmitted field was less than 0.5%.

	Desired Field Polarization		
Antenna	X	Y	Z
Horizontal	Passed	Failed	Failed
Vertical	Failed	Passed	Failed

The signal generator and the E-field probe introduce error into the test. The main errors caused by the signal generator are fluctuations in the frequency being produced, noise and level errors. These errors are insignificant with respect to the error caused by the E-field probe. The probe has error with respect to frequency response and level response. For the 10 V/m used in this test, the probe has a linearity of ±0.5 dB. The frequency response of the probe is ±0.5 dB for 100 kHz to 100 MHz and ±1.4 dB for 100 MHz to 3 GHz.

The results of the simple test outlined in this document show that the system as a whole is capable of generating the desired field in the desired dimension at the desired frequency when the parameters of the test fall within the specifications of the test setup.

References

1. C. E. Baum, *Interaction Notes* **400** (1980); also in *Proc. Zurich EMC Symp.*, 209-214 (1982).
2. J. P. Parmantier, V. Gobin, F. Issac, I. Junqua, Y. Daudy, and J. M. Lagarde, *Interaction Notes* **506**, (1993).
3. J. E. Nanevicz, E. F. Vance, W. Radasky, M. A. Uman, G. K. Soper, and J. M. Pierre, *IEEE Trans. Electromagn. Compat.*, **30**(4), 463-472 (1988).
4. A. K. Agrawal, H. J. Price, and S. H. Gurbaxani, *IEEE Trans. Electromagn. Compat.*, **22**, pp. 119-129 (1980).
5. K. S. Yee, *IEEE Trans. Antennas Propagat.*, **AP-14(3)**, pp. 302-307 (1966).
6. P. Kirawanich, N. Kranthi, R. Gunda, A. R. Stillwell, and N. E. Islam, *J. Appl. Phys.*, **96** (10), (2004).
7. P. B. Johns and R. L. Beurle, *Proc. Inst. Elec. Eng.*, **118**, 1203 (1971).
8. D. Johns and C. Christopolos, *IEE Proc.-Sci. Meas. Technol.*, **141**(4), 310 (1994).
9. B. Archambeault, C. Brench, and O. M. Ramahi, EMI/EMC Computational Modeling Handbook, 2nd Ed. (Kluwer Academic Publishers, 2001).
10. C. Christopoulos, The Transmission-Line Modeling Method TLM, (IEEE Press, 1995).

11. M. N. O. Sadiku, Numerical Techniques in Electromagnetics, 2nd Ed. (CRC Press LCC, 2001).
12. Eswarappa, G. I. Costache, and W. J. R. Hoefer, *IEEE Trans. Microwave Theory Tech.*, **38**(4), 379 (1990).
13. J. P. Parmantier and P. Degauque, *Modern Radio Sci.*, 151 (1996).
14. Z. Chen, M. M. Ney, and W. J. R. Hoefer, *IEEE Trans. Microwave Theory Tech.*, **39**(3), 377 (1991).
15. H. A. Bethe, *Phys. Rev.*, **66**(7), (1994).
16. O. Mitrofanov, M. Lee, J. W. P. Hsu, L. N. Pfeiffer, K. W. West, and J. D. Wynn, *Appl. Phys. Lett.*, **79**(7), (2001).
17. C. R. Paul and J. W. McKnight, *IEEE Trans. Electromagn. Compat.*, EMC-21(2), 92–105 (1979).
18. C. R. Paul and J. W. McKnight, *IEEE Trans. Electromagn. Compat.*, EMC-21(2), 105–114 (1979).
19. J. P. Parmantier and J. P. Aparicio, *Proc. Zurich EMC Symp.*, Zurich, Switzerland, 12-14 March (1991).
20. C. E. Baum, *Interaction Notes* **478**, Kirtland, New Mexico, USA (1989).
21. J. C. Clements, C. R. Paul, and A. T. Adams, *IEEE Trans. Electromagn. Compat.*, EMC-17(4), 238–248 (1975).
22. N. E. Islam, E. Schamiloglu, C. B. Fleddermann, J. S. H. Schoenberg, and R. P. Joshi, *Intl. conference on Plasma Science*, **1**, June 1999.
23. F. La Via, F. Roccaforte, A. Makhtari, V. Raineri, P. Musumeci, and L. Calcagno, *Microelectronic Engineering*, **60**, 269-282 (2002).
24. ATLAS User's Manual, SILVACO International.
25. S. K. Ghandhi, Semiconductor power devices: physics of operation and fabrication technology, New York : Wiley, c1977.
26. User Manual, CST Microwave Studio 5.0 (2005).
27. H. S. Nalwa, Photodetectors and Fiber Optics, (Academic Press, 2001).
28. N. S. Kranthi, M. O. Nizam, P. Kirawanich, N. E. Islam, A. K. Sharma, and S. L. Lucero, *Appl. Phys. Lett.*, **87**(24), (2005).
29. G. Kristensson, *PIER*, **55**, 1-31 (2005).

V. PERSONNEL SUPPORTED

1. Phumin Kirawanich (Postdoctoral Fellow, INS permission to work in US)
2. Rahul Gunda (Graduated)
3. Nakka S. Kranthi (Graduated)
4. Sravanthi Kache (Graduated)
4. Jeffery C. Kroenung (US national)
5. Andrew R. Stillwell (US national, till last semester)
6. Ryan Furtado (US national)
7. George Ball (US national, summer)
8. Tim Evans (US national, summer)
9. David S. Gleason (US national)
10. Robert Feldhaus (US national)
11. Bennet Yannuzzi (US national, summer)
12. David Mueller (US national)
13. Justin Ross (US national)
14. Gena Belgarde(US national)
15. Ashkan Seyedi (US national)
16. Anthony Cornell (US national)
17. Waseem Akbar (supported)
18. Mohammad O. Nizam (supported)
19. Pavan K. Gummadavalli (unsupported)
20. Nikhil Parsi (unsupported)
21. Jesse Simpson (US national, summer)

VI. PUBLICATIONS

Year 2006

Book Articles

[2006B1] Phumin Kirawanich, Nakka S. Kranthi, Rahul Gunda, Jean-Philippe Parmantier, Solange Bertuol, and N. E. Islam, Simulating the response of semi-shielded systems: electromagnetic topology technique, Ultra-Wideband Short-Pulse Electromagnetics 7, Kluwer Academic Publishers, expected 2006.

Journal Publications

[2006J1] P. Kirawanich, N. E. Islam, and S. J. Yakura, "An electromagnetic topology approach: crosstalk characterizations of the unshielded twisted-pair cable," *Progress In Electromagnetics Research*, J. A. Kong (ed.), PIER 58, pp. 285-299, 2006.

[2006J2] Rahul Gunda, David Gleason, Kapil Kelkar, Phumin Kirawanich, William C. Nunnally, and N. E. Islam, "Radiofrequency heating of photoconductive switch for high power applications," *IEEE Transactions on Plasma Sciences*, the 2006 special issue (submitted).

[2006J3] P. Kirawanich, D. Gleason, and N. E. Islam, "An electromagnetic topology and transmission line hybrid solution to aperture interactions," *Journal of Applied Physics* (revised).

[2006J4] Sravanthi Kache, Nakka S. Kranthi, M. O. Nizam, Phumin Kirawanich, R. W. McLaren, A. K. Sharma, S. L. Lucero, and N. E. Islam, "Field analysis to optimize charge collection in a sub-micron grated metal-semiconductor-metal photodetector," *Journal of Applied Physics* (submitted).

Reviewed Conference Publications

[2006C1] Phumin Kirawanich, David Gleason, S. Joe Yakura, and N. E. Islam, "Crosstalk characterizations of an unshielded twisted-pair cable in an electrical large system using the electromagnetic topology concept," Proceedings of the 17th International Zurich Symposium on Electromagnetic Compatibility, Feb. 27- Mar. 03, 2006, Singapore (accepted).

Year 2005

Book Articles

[2005B1] F. J. Agee, P. Kirawanich, J. Yakura, G. Tzeremes, C. Christodoulou, and N. E. Islam, An electromagnetic topology based simulation for aperture interactions using transmission lines as radiating elements, Computational Methods and Experimental Measurements XII, Wessex Institute of Technology Transactions on Modelling & Simulation (ISSN 1743-355X), vol 41, pp. 94, 2005.

Journal Publications

[2005J1] Nakka S. Kranthi, M. O. Nizam, Phumin Kirawanich, Naz E. Islam, A. K. Sharma, and S. L. Lucero, "Fields analysis of enhanced charge collection in nanoscale grated photo detectors," *Applied Physics Letters*, vol. 87, no. 24, Dec. 2005.

[2005J2] Phumin Kirawanich, Nakka Kranthi and N. E. Islam, "Electromagnetic topology based analysis of coupling through small aperture on cables of communication systems," *Electromagnetics*, the special issue on "RF Effects on Digital Systems: Part I", vol. 25, no. 7-8, pp. 589-602, Oct.-Dec. 2005.

[2005J3] Phumin Kirawanich, George Tzeremes, Christos Christodoulou, S. Joe Yakura, and N. E. Islam, "Electromagnetic wave penetrating through apertures: Comparison of

electromagnetic topology technique with FDTD method," *Antennas and Wireless Propagation Letters*, vol. 4, no. 15 , pp. 151-154, 2005.

Reviewed Conference Publications

[2005C1] S. Joe Yakura, Phumin Kirawanich, David Gleason, and N. E. Islam, "Application of transmission line matrix methodology to electromagnetic topology simulations for EMP penetration through apertures," the International Conference on Electromagnetics in Advanced Applications and European Electromagnetic Structures Conference, ICEAA '05 and EESC '05, Sep. 12-16, 2005, Torino, Italy.

[2005C2] Phumin Kirawanich, David Gleason, Anthony Cornell, and N. E. Islam, "Analysis of field through apertures by applying transmission line matrix method to electromagnetic topology simulations," Proceedings of the 2005 IEEE Electromagnetic Compatibility Symposium, Aug. 8-12, 2005, Chicago, Illinois, USA.

[2005C3] Phumin Kirawanich, David Gleason, and N. E. Islam, "Simulations for high power microwave penetration through apertures: application of transmission line matrix methodology to electromagnetic topology," Abstract at the 32nd IEEE International Conference on Plasma Science, ICOPS 2005, 18-23 June 2005, pp. -, Monterey, California, USA.

[2005C4] Rahul Gunda, Phumin Kirawanich, and N. E. Islam, "Effects of heating on Photoconductive Semiconductor switches: simulation and analysis," Proceeding of the 15th IEEE International Pulsed Power Conference, PPC 2005, 13-17 June 2005, pp. -, Monterey, California, USA.

[2005C5] Phumin Kirawanich, David Gleason, and N. E. Islam, "An electromagnetic topology and transmission line matrix hybrid technique for modeling high power electromagnetic interactions," Proceeding of the 15th IEEE International Pulsed Power Conference, PPC 2005, 13-17 June 2005, pp. -, Monterey, California, USA.

[2005C6] Forrest J. Agee, Phumin Kirawanich, S. Joe Yakura, George Tzeremes, Christos Christodoulou, and N. E. Islam, "An electromagnetic topology based simulation for aperture interactions using transmission lines as radiating elements," 12th International Conference on Computational Methods and Experimental Measurements (CMEM 2005), 20-22 June 2005, Malta.

[2005C7] Phumin Kirawanich, Nakka S. Kranthi, A. R. Stillwell, Forrest J. Agee, S. Joe Yakura, and N. E. Islam, "Analysis of the wire coupling under an aperture illuminated by an incident field by means of a topological approach," Proceedings of the 16th International Zurich Symposium on Electromagnetic Compatibility, Feb. 13-18, 2005, Zurich, Switzerland.

Year 2004

Journal Publications

[2004J1] George Tzeremes, Phumin Kirawanich, Christos Christodoulou, and N. E. Islam, "Transmission lines as radiating antenna in sources aperture interactions in electromagnetic topology simulations," *Antennas and Wireless Propagation Letters*, vol. 3, no. 15 , pp. 283-286, Dec. 2004.

[2004J2] Phumin Kirawanich, Nakka Kranthi, Rahul Gunda, and N. E. Islam, "An electromagnetic topology based susceptibility analysis of cables in aircrafts and shielded systems," *Journal of Applied Physics*, vol. 96, no. 10, pp. 5892-5897, Nov.15, 2004.

[2004J3] Phumin Kirawanich, Nakka S. Kranthi, Jeffery C. Kroenung and N. E. Islam, "Methodology for interference analysis using electromagnetic topology techniques," *Applied Physics Letters*, vol. 84, no. 15, pp. 2949-2951, Apr. 12, 2004.

Reviewed Conference Publications

[2004C1] Phumin Kirawanich, Nakka S. Kranthi, and N. E. Islam, "Modeling External Interference on Systems Using Electromagnetic Topology Technique," Proceedings of the 2004 IEEE Electromagnetic Compatibility Symposium, EMC 2004, vol. 3, Aug 9-13, 2004, pp. 804-808, Santa Clara, California, USA.

[2004C2] Phumin Kirawanich, Nakka S. Kranthi, Rahul Gunda, Jean-Philippe Parmantier, Solange Bertuol, and N. E. Islam, "Simulating the Response of Semi-Shielded Systems: Electromagnetic Topology Technique," EUROEM-2004, July 12-16, 2004, Magdeburg, Germany.

[2004C3] Phumin Kirawanich, Rahul Gunda, Nakka Kranthi, and N. E. Islam, "Network Cables Under Lightning Pulse: Electromagnetic Topology Analysis," Abstract at the 31st IEEE International Conference on Plasma Science, ICOPS 2004, 28 June-1 July 2004, pp. 374, Baltimore, Maryland, USA.

[2004C4] Phumin Kirawanich, Rahul Gunda, Nakka Kranthi, and N. E. Islam, "Electromagnetic Topology Analysis: Small Apertures and Lightning Interactions," Abstract at the 2004 IEEE Antennas and Propagation Society Symposium, vol. 4, 20-25 June 2004, pp. 3859-3862, Monterey, California, USA.

[2004C5] Jack Agee, Phumin Kirawanich, Rahul Gunda, Nakka Kranthi, Jeffery Kroenung and N. E. Islam, "Electromagnetic topology technique for system interaction through small apertures," Proceedings of the 2004 IEEE International Symposium Electromagnetic Compatibility, Jun. 1-4, 2004, Sendai, Japan.

VII. INTERACTIONS/TRANSITIONS

Conferences, meetings, and symposium

We have actively participated in several EMC-related symposiums, meetings and conferences, and contributed by giving presentation.

1. The 2005 IEEE Electromagnetic Compatibility Symposium, Chicago, Illinois, USA, Aug. 8-12, 2005.
   Title: *Analysis of field through apertures by applying transmission line matrix method to electromagnetic topology simulations.*
2. The 32nd IEEE International Conference on Plasma Science, ICOPS 2005, Monterey, California, USA, June 18-23, 2005.
   Title: *Simulations for high power microwave penetration through apertures: application of transmission line matrix methodology to electromagnetic topology*
3. The 15th IEEE International Pulsed Power Conference, PPC 2005, Monterey, California, USA, June 13-17, 2005.
   Title: *Effects of heating on Photoconductive Semiconductor switches: simulation and analysis*
4. The 15th IEEE International Pulsed Power Conference, PPC 2005, Monterey, California, USA, June 13-17, 2005.
   Title: *An electromagnetic topology and transmission line matrix hybrid technique for modeling high power electromagnetic interactions*
5. The 16th International Zurich Symposium on Electromagnetic Compatibility, Zurich, Switzerland, Feb. 13-18, 2005.
   Title: *Analysis of the wire coupling under an aperture illuminated by an incident field by means of a topological approach," Proceedings of the 16th International Zurich Symposium on Electromagnetic Compatibility*
6. The 2004 IEEE EMC Symposium, Santa Clara, California, USA, Aug 9-13, 2004.
   Title: *Modeling External Interference on Systems Using Electromagnetic Topology Technique*
7. IEEE International Conference on Plasma Science, Baltimore, Maryland, USA, June 28-July 1st, 2004
   Title: *Network Cables under Lightning Pulse: Electromagnetic Topology Analysis.*

8. The 2004 IEEE APSURSI International Symposium on Antennas and Propagation and USNC/URSI National Radio Science Meeting, Monterey, California, USA, June 20-26, 2004.
   Title: *Electromagnetic Topology Analysis: Small Apertures and Lightning Interactions*
9. The 2004 International Symposium Electromagnetic Compatibility, SENDAI, Japan, June 1-4, 2004.
   Title: *Electromagnetic topology technique for system interaction through small apertures*

Classified Presentation

Collaborations include regular exchange of data, visits and co-authoring of research papers at the national and international forum (Sendai-Japan, June 1-4, 2004, Zurich-Switzerland, Feb 13-18, 2005, Magdeburg, Germany, July 12-16 2004, and Torino-Italy, Summer, 2005 and journal publications. It also included the following special sessions:

- The Five-power Air Senior National Representative (ASNR) High Power Microwave Meeting, held 14-17 February 2005 at Eglin AFB, FL. The meeting is held every six months either in the US or Europe, alternating the location every six months. The five-power nations consist of the senior government officials from USA, the UK, Germany, France and Italy. Since Italy just became a member last year, Italy has not yet sent anybody to the meeting. The purpose of this group is to share the information and establish international collaboration on HPM research among participating nations.

  The title of the paper presented is "Analysis of the Wire Coupling under an Aperture Illuminated by an Incident Field by Means of a Topological Approach."

  The authors are S. Joe Yakura (AFRL/DEHE), Phumin Kirawanich (U of Missouri at Columbia), Nakka S. Kranthi (U of Missouri at Columbia), A. R. Stillwell (U of Missouri at Columbia), N. E. Islam (U of Missouri at Columbia), and Forrest J. Agee (AFOSR).

- Directed Energy Professional Society (DEPS) High Power Microwave Conference (classified), held 17-19 August 2004 in Albuquerque, NM. This conference covers the

progress in the development and application of high power microwave (HPM) technologies for directed energy missions. It suggests that it is time for DEPS to sponsor a conference specifically devoted to HPM. Re-establishment of a common perspective on HPM missions and potential directions requires the appropriate security level and the attendance of the relevant experts and managers. This conference is classified SECRET. Attendance was limited to U.S. citizens with secret or higher security clearances.

Paper title "Approximated Non-uniform Baum-Liu-Tesche (BLT) Formulation of Transmission-line Theory for One-wire Network Systems."

Authors are S. Joe Yakura (AFRL/DEHE) N. E. Islam (Univ. of Missouri at Columbia) and P. Kirawanich (Univ. of Missouri at Columbia).

Consultative and advisory functions to laboratories and agencies

We have established close, interactive research collaboration with the Directed Energy Directorate, AFRL, NM. This collaboration is an extension of our previous efforts when the PI for this project was at the University of New Mexico, NM. Collaborations include frequent exchange of information regarding usage and models for the CRIPTE code and providing upgrades to the CRIPTE manual that has been electronically transmitted to Dr. Joe Yakura, who is in charge of the CRIPTE simulations at DE, AFRL. The models developed so far and the associated circuitry has been sent to Dr. Yakura who is expected to use it for his research work at AFRL, NM. The latest version of the code has also been transmitted to AFRL, for use by Dr. Yakura and his group.

Whenever required we have provided the necessary help for the AFRL group to understand the inner workings of the code and have consulted the group to setup small scale experiments at U Missouri-Columbia. Experiments will be conducted at the U Missouri-Columbia laboratories.

Transitions

The techniques we have established for external-internal interactions through an aperture for EMC/EMI studies can be utilized for aircraft cable or other sensitive military hardware. We expect Dr. Yakura at DE/AFRL, NM to conduct research in this area.

VIII. NEW DISCOVERIES

1. We have reported, for the first time, a process for the generation and use of transfer functions for topological simulations. This function is critical in topological simulations where external electromagnetic pulses interact with electrical systems through an aperture. Previously measured transfer function was used in analysis.

2. We propose a simpler and accurate methodology, which combines the EMT approach with the transmission line matrix (TLM) method to account for the coupling of an incident electromagnetic field with an aperture over an infinite metallic plane in a topological simulation setting.

3. Based on EMT analysis, the straight-through, differential-generator, twisted-pair receptor model is the most effective configuration to control the near-end crosstalk level, due to the influence from both the neutralizing mutual inductance and the single current generator.

4. Through RF interactions if the anode is heated to 330 K, a current controlled negative resistance characteristic occur in both GaAs and SiC PCSS. Current filamentation forces the devices to breakdown at a much lower voltage, which is more severe in SiC material. For SiC, better thermal conductivity allows for fast heat dissipation throughout the device and in the absence of a heat sink the temperature increase results in local thermal carrier generation at a voltage that is much less as compared to a GaAs PCSS. Negative resistivity-like behavior leading to unstable filamentation and thermal runaway is expected to be more severe in SiC.

5. Charge collection in a MSM photo detector can be studied by tracing the amplitude of the transmitted E-field into the active region of the detector. An increase in the transmitted E-field amplitude means an increase in the transmission coefficient. The transmission coefficient determines the energy carried by the transmitted wave into the detector's active region. Simulations show that collection in MSM detectors can be improved by adding gratings in the active region. Simulations also show that the energy deposited in the active region depends on the shape and height of the gratings. This indirectly affects the charge collection of the photodetector.

IX. HONORS/AWARDS

1. Was nominated for and granted IEEE senior membership for recent accomplishments which including research work for the AFOSR supported project.
2. Recipient of research grant of $173,000 for the test chamber to perform an electromagnetic conducted and radiation susceptibility tests.

X. ACKNOWLEDGEMENT

We sincerely acknowledge the advice and support extended to us by Bill Prather, Dr. Joe Yakura, and Dr. Mike Harrison at DEHE, AFRL, NM.